HHS Public Access

Author manuscript

Nature. Author manuscript; available in PMC 2021 August 15.

Published in final edited form as:

Nature. 2021 March ; 591(7851): 645–651. doi:10.1038/s41586-020-03045-2.

Metabolic support of tumor-infiltrating regulatory T cells by lactic acid

McLane J. Watson[1,2,3], **Paolo D.A. Vignali**[1,2,3], **Steven J. Mullett**[4], **Abigail E. Overacre-Delgoffe**[1,5], **Ronal M. Peralta**[1,2,3], **Stephanie Grebinoski**[1,3], **Ashley V. Menk**[2], **Natalie L. Rittenhouse**[5], **Kristin DePeaux**[1,2,3], **Ryan D. Whetstone**[1,2], **Dario A. A. Vignali**[1,2,6], **Timothy W. Hand**[5,6], **Amanda C. Poholek**[5], **Brett M. Morrison**[7], **Jeffrey D. Rothstein**[7], **Stacy G. Wendell**[4,8], **Greg M. Delgoffe**[1,2,6,*]

[1]Department of Immunology, University of Pittsburgh, Pittsburgh, PA, USA

[2]Tumor Microenvironment Center, UPMC Hillman Cancer Center, Pittsburgh, PA, USA

[3]Graduate Program of Microbiology and Immunology, University of Pittsburgh School of Medicine, Pittsburgh, PA, USA

[4]Health Sciences Metabolomics and Lipidomics Core, University of Pittsburgh, Pittsburgh, PA, USA

[5]Department of Pediatrics, UPMC Children's Hospital of Pittsburgh, Pittsburgh, PA, USA

[6]Cancer Immunology and Immunotherapy Program, UPMC Hillman Cancer Center, Pittsburgh, PA, USA

[7]Department of Neuroscience, Johns Hopkins University School of Medicine, Baltimore, MD, USA

[8]Departments of Pharmacology and Chemical Biology and Clinical Translational Science, University of Pittsburgh, Pittsburgh, PA, USA

SUMMARY

Regulatory T (T_{reg}) cells, vital for maintaining immune homeostasis, also represent a major barrier to cancer immunity, as the tumor microenvironment (TME) promotes T_{reg} cell recruitment, differentiation, and activity[1,2]. Tumor cells have deregulated metabolism leading to a metabolite-depleted, hypoxic, and acidic TME[3], placing infiltrating effector T cells in competition with tumors for metabolites, impairing their function[4–6]. Conversely, T_{reg} cells maintain high

*Correspondence and requests for materials should be addressed to gdelgoffe@pitt.edu.

Author Contributions

MJW performed the majority of the experiments, analyzed data, and wrote the manuscript. PDAV helped perform isotopic flux analysis, suppression assays, and contributed to writing, SJM performed and analyzed isotopic flux analysis, AEOD performed all the transfer colitis experiments, RMP performed in vitro differentiation and suppression assays, SG helped purify and analyze cells from NOD mice, AVM performed extracellular flux analysis and tumor histology analysis, NLR analyzed RNAseq data, KD performed various in vitro experiments, RDW sorted cells for isotopic flux and RNA sequencing, DAAV provided *Foxp3*$^{\text{FlpO-Ametrine}}$, NOD.Foxp3GFP mice and scientific insight, BMM and JDR generated and provided the *Slc16a1*$^{f/f}$ mouse and scientific insight, TWH provided insight and facilities for transfer colitis experiments, ACP helped perform and analyze RNAseq data, SGW oversaw analysis of isotopic flux data, and GMD conceived of the study, performed initial experiments, obtained funding, and wrote the manuscript.

The authors declare no competing interests.

suppressive function within the TME[7,8]. As previous studies suggested T_{reg} cells possess a distinct metabolic profile from effector T cells[9–11], we hypothesized the altered metabolic landscape of the TME and increased activity of intratumoral T_{reg} cells are linked. Here we show T_{reg} cells display broad heterogeneity in utilization of glucose metabolism within normal and transformed tissues and can engage an alternative metabolic pathway to maintain suppressive function and proliferation. Glucose uptake correlated with poorer suppressive function and long-term instability, and high glucose culture impaired T_{reg} cell function and stability. T_{reg} cells rather upregulate pathways in metabolism of the glycolytic byproduct lactic acid. T_{reg} cells withstood high lactate conditions, and lactate treatment prevented the destabilizing effects of high glucose, generating intermediates necessary for proliferation. T_{reg} cell-restricted deletion of MCT1, a lactate transporter, revealed lactate uptake is dispensable for peripheral T_{reg} cell function but required intratumorally, resulting in slowed tumor growth and increased response to immunotherapy. Thus T_{reg} cells are metabolically flexible: they can utilize 'alternative' metabolites in the TME to maintain suppressive identity. Further, our studies suggest tumors avoid destruction by not only depriving effector T cells of nutrients, but also metabolically supporting regulatory populations.

T_{reg} cells thrive under glucose restriction

Having previously shown heightened tumor cell metabolism correlates with decreased effector T cell function[5], we sought to determine the relationship of heighted tumor metabolism with T_{reg} cell function. We measured the suppressor activity of T_{reg} cells isolated from *Foxp3* reporter mice[12,13] bearing tumors of increasing glycolytic capacity, revealing glycolysis of tumor cells correlated with suppressive function of intratumoral T_{reg} cells (Fig. 1a). Expectedly, T_{reg} cells were enriched within tumors (Fig. 1b, Extended Data Fig. 1a,b) and were not metabolically suppressed but actively proliferating (Fig. 1c). Given the relationship between tumor glycolysis and T_{reg} cell function, we determined the glycolytic capacity of T_{reg} cells directly *ex vivo* and immediately after activation, a reprogramming event occurring downstream of the TCR in T cells[14]. TCR triggering induced less glycolysis in T_{reg} cells compared to naïve or antigen-experienced conventional T cells (Fig. 1d). This resistance to glycolysis persisted under strong activating stimuli (anti-CD3, CD28, and IL-2 for 48 h), and tumor-derived T_{reg} cells displayed even lower glycolytic activity (Extended Fig. 1c). Oligomycin treatment showed T_{reg} cells are resistant to engaging glycolysis even when oxidative metabolism is inhibited, suggesting glucose transport may be limiting in T_{reg} cells (Extended Data Fig. 1c). Indeed, T_{reg} cells had significant reductions in glucose uptake based on the fluorescent glucose tracer 2NBDG compared to T_{conv} ($CD4^+$ $Foxp3^-$) cells directly *ex vivo* (Fig. 1e, Extended Data Fig. 1d), regardless of CD44/CD62L expression (notably, the largest difference was observed between $CD62L^{hi}$ populations) (Extended Data Fig. 1e). To directly compare activation-induced T_{reg} and T_{conv} glucose uptake, we adoptively transferred congenically marked OT-II $CD4^+$ T cells from *Foxp3*^{RFP} mice into *Vaccinia*^{OVA}-infected hosts. OT-II T_{reg} cells took up significantly less 2NBDG than their $Foxp3^-$ counterparts, despite sharing the same TCR and undergoing robust activation (Fig. 1f). While not selected on the OT-II TCR, activation by the same antigen *in vivo* under the same inflammatory context results in disparate metabolic phenotypes if Foxp3 is expressed.

To determine if low glucose uptake was a universal phenotype of T_{reg} cells, we interrogated the infiltrate of various tissues at normal and inflammatory states . 2NBDG is not only incompatible with YFP and GFP employed in *Foxp3*-driven Cre lines, but may have limited utility in some cells as a glucose tracer[16]. Thus, we synthesized a novel fluorescent glucose tracer (Cy5-linked 1amino-glucose; GlucoseCy5[17]), recapitulating our findings with 2NBDG while demonstrating superior specificity and sensitivity (Extended Data Fig. 1f–h). T_{reg} cell glucose uptake was quite heterogeneous in tissues of *Foxp3*^{YFP}-iCre mice, but notably low in B16 and imiquimod-inflamed skin (Fig.1g), suggesting inflammation may drive lower glucose uptake in T_{reg} cells. Conventional T cells possessed far less heterogeneity in glucose avidity when assayed from the same environments (Extended Data Fig. 1i).

Glucose avidity predicts T_{reg} cell function

We next purified T_{reg} subsets of low and high glucose avidity and measured their function. Regardless of tissue, 2NBDG avid T_{reg} cells displayed significantly reduced suppressive capacity compared to 2NBDG^{lo} T_{reg} cells (Fig. 2a, Extended Data Fig 2a), not attributable to viability, as 2NBDG^{hi} T_{reg} cells were rather more viable after the assay (Extended Data Fig 2b,c), and retained their initial proclivities for glucose (Extended Data Figure 2b,d). Thus, within a tissue, avidity for glucose predicts poorly suppressive T_{reg} cells. Sequencing 2NBDG low and high LN and B16-infiltrating T_{reg} cells revealed reduced expression of *Foxp3*, *Ikzf2* (Helios), *Il2ra* (CD25), *Nrp1*, and other T_{reg} signature genes in 2NBDG^{hi} T_{reg} cells, further confirmed by flow cytometry (Fig. 2b, Extended Data Fig. 2e). These data suggested while glucose avid T_{reg} cells are still Foxp3^{+}, they harbor a ‘weaker’ T_{reg} cell signature. As 2NBDG^{hi} T_{reg} cells harbored some suppressor function, we measured cytokine production after a brief restimulation. 2NBDG^{hi} T_{reg} cells produced significantly more IL-10, suggesting distinct suppressive mechanisms between 2NBDG T_{reg} states, especially intriguing given the differences in mRNA (Fig. 2b,c). These differences may be driven by glycolysis which is tied to cytokine translation in conventional T cells[18]. To assess long-term stability and function of 2NBDG T_{reg} cell subsets under inflammation, Thy1.2^{+} Foxp3^{+} T_{reg} cells of high or low glucose avidity were transferred into *Rag1*-deficient animals, along with Thy1.1^{+} Foxp3^{-} T_{conv} cells to induce colitis. After 12 weeks, mice receiving glucose avid T_{reg} cells began to lose weight due to increased colitis compared to those receiving 2NBDG^{lo} T_{reg} cells, and transferred 2NBDG^{hi} T_{reg} cells lost *Foxp3* expression (**Fig. 2d,e, Extended Data Fig. 2f**). We also investigated whether increased glucose uptake could be observed in T_{reg} cells from an unmanipulated autoimmune setting. T_{reg} cells isolated from pancreatic islets (known to be dysfunctional[19]) and draining lymph node of pre-diabetic NOD.*Foxp3*^{GFP} mice took up significantly more glucose than those from non-draining lymph node (ndLN) (Fig. 2f). Thus, glucose avidity in T_{reg} cells correlates with poor suppressive capacity, ultimately leading to instability.

We next asked whether exposure to a high glucose environment would drive a less suppressive phenotype, regardless of glucose uptake status. Remarkably, conditioning T_{reg} cells in high glucose dampened suppressive function when later assayed in isoglycemic conditions (Fig. 2g, Extended Data Fig. 2g). We further interrogated the transcriptome of 2NBDG^{lo} T_{reg} cells to identify metabolic pathways that may support their function.

2NBDG^{lo} T_{reg} cells did not possess a transcriptome suggesting preferential lipid metabolism; rather, lipid metabolism genes were enriched in the 2NBDG^{hi} subset (Extended Data Fig. 2h). Both subsets expressed upstream enzymes in glycolysis, suggesting proclivity for glucose was not regulated at the level of transporter or enzyme expression (Fig. 2h). The 2NBDG^{lo} subpopulation, however, had enriched expression for the terminal steps of glycolysis: specifically lactate dehydrogenase (*Ldha*), and the monocarboxylate transporter MCT1 (encoded by *Slc16a1*) (Fig. 2h), confirmed by qPCR (Extended Data Fig 2i). While lactate is the end-product of glycolysis, it represents a significant fuel source for many cells[20]. Lactate uptake is mediated through MCT1, where it is converted by LDH to pyruvate[21]. T_{reg} cells (but not T_{conv} cells) conditioned in low or glucose-deficient media increased expression of *Ldh*a and *Slc16a1* (Extended Data Fig. 2j). Thus, T_{reg} cells upregulate genes involved in lactate metabolism.

T_{reg} cells can metabolize lactic acid

Lactic acid is highly enriched in the TME[22] (Fig. 3a) and known to be immunosuppressive[23,24], and, indeed, it curbed function of conventional T cells *in vitro* (Extended Data Fig. 3a,b). Conversely, both T_{reg} cell suppressor function and proliferation were resistant to tumor-equivalent concentrations of lactic acid (Extended Data Fig. 3a,c). Lactate can stimulate cells via GPR81[25] and enter as a metabolite via MCT1, so we asked if T_{reg} cells could consume lactic acid by measuring pH changes[26]. Lymphocytes from *Foxp3$^{YFP\text{-}Cre}$* reporter mice were loaded with intracellular pH dye and incubated with lactic acid. T_{reg} cells, but not T_{conv} cells, took up lactic acid, evidenced by increased fluorescence (Fig. 3b). This assay revealed lactic acid uptake was also heterogeneous within various tissue-derived T_{reg} cells, akin to analysis of glucose uptake, notably low in tissues where T_{reg} cells were glucose avid, such as the liver (Fig. 1g, 3c). Indeed, most dye+ T_{reg} cells did not take up glucose (Extended Data Fig. 3d). In autoimmune NOD mice, islet T_{reg} cells took up less lactic acid than those from the ndLN or pLN (Fig. 3d). pH dye+ T_{reg} cells from LN and B16 TIL possessed increased CD44 and Nrp1 expression, while maintaining similar Foxp3 expression to dye negative cells (Fig. 3e). Thus T_{reg} cells are not only resistant to lactic acid but can take up this metabolite, and those that do display an activated T_{reg} cell signature and low glucose uptake.

To identify how T_{reg} cells were utilizing lactic acid, we performed high resolution mass spectrometry on activated T_{reg} and T_{conv} cells pulsed with [U^{13}C]-L-lactate (at pH 6.9) (Fig. 3f). We used LN-derived T_{reg} cells (which do readily take up lactate, Fig. 3b) to facilitate cellular input needed for MS analysis, confirming T_{reg} cells took up significantly more lactate than T_{conv} cells (Fig. 3g). T_{reg} cells converted ^{13}C-lactate into pyruvate and subsequently into citrate and malate indicating mitochondrial import and entry to the TCA cycle (Fig. 3g). Further analysis ~~of~~ revealed T_{reg} cells also incorporated lactate-derived carbon into phosphoenolpyruvate (PEP) (Fig 3h), formed by phosphoenolpyruvate carboxykinase (PEPCK) when malate leaves the mitochondria and is converted to oxaloacetate. PEP can contribute to upstream glycolytic intermediates essential for proliferation, suggesting lactate may serve as a gluconeogenic fuel source, decreasing a T_{reg} cell's need for glucose. As high glucose can inhibit T_{reg} cell suppressor function (Fig. 2g), we asked whether lactic acid could mitigate the deleterious effects of glucose. Indeed,

conditioning T_{reg} cells in high glucose plus tumor-equivalent concentrations of lactic acid maintained suppressor function (Fig 3i).

We then used the PEPCK inhibitor 3-mercaptopicolinic acid (3MP)[27] to dissect the individual contributions of lactate uptake and oxidation from upstream gluconeogenic reactions dependent on lactate-derived PEP. 3MP treatment of ^{13}C-lactate pulsed T_{reg} cells reduced PEP accumulation without impacting incorporation into the TCA cycle (Fig 3j). *In vitro* 3MP treatment of T_{reg} cells in lactic acid significantly reduced their proliferation (Extended Data Fig. 3i). However, 3MP did not impact suppressive capacity of T_{reg} cells in vitro (Extended Data Fig. 3j). Treating tumor-bearing mice with 3MP decreased proliferation of tumor-resident, but not LN, T_{reg} cells, and increased intratumoral CD8 IFN-γ production (Fig. 3k,l). However, it did not overtly affect the intratumoral percentage of Foxp3$^+$ cells, T_{conv}/CD8:T_{reg} cells ratios, overt tumor growth, or suppressor function when interrogated *ex vivo* (Extended Data Fig. 3f–h). Thus T_{reg} cells utilize lactic acid to not only feed the TCA cycle, but to generate PEP, critical for fueling T_{reg} cell proliferation within the tumor.

Lactic acid supports intratumoral T_{reg} cells

To determine the significance of lactic acid utilization by T_{reg} cells *in vivo*, we generated a constitutive, T_{reg}-specific deletion of MCT1 (*Slc16a1*$^{f/f}$*Foxp3*^{Cre}). qPCR confirmed *Slc16a1* deletion, lack of compensation by *Slc16a7*/MCT2 or *Slc16a3*/MCT4 upregulation, and no deletion in CD4$^+$Foxp3$^-$ cells (Extended Data Fig. 4a,b). Expectedly, deletion of *Slc16a1* resulted in loss of lactic acid uptake (Fig. 4a). These mice did not show any overt signs of autoimmunity or lymphoproliferation (Extended Data Fig. 4c,d). Rather, T_{reg} cells from the LN of *Slc16a1*$^{f/f}$*Foxp3*^{YFPCre} mice displayed similar suppressive capacity, proliferation, and expression of T_{reg} signature genes when assayed *ex vivo* (Extended Data Fig. 4e–h). MCT1 deficiency in T_{reg} cells revealed no significant differences in percentage of Foxp3$^+$ cells infiltrating various tissues, although several compartments showed increases in glucose uptake at the steady-state (Extended Data Fig. 4i,j). Imiquimod treatment resulted in no increased inflammatory ear thickness, nor loss of T_{reg} cell markers in *Slc16a1*$^{f/f}$*Foxp3*^{Cre} mice (Extended Data Fig. 4k,l). We also determined long-term function and stability of MCT1-deficient T_{reg} cells in transfer colitis. Unlike 2NBDG^{hi} T_{reg} cells, MCT1-deficient T_{reg} cells did not show reduced stability (Extended Data Fig. 4m). However, they were not completely functional: at 7 weeks, mice receiving MCT1-deficient T_{reg} cells had more histologically severe colitis, although less severe than mice receiving 2NBDG^{hi} T_{reg} cells (Extended Data Fig. 4n,o). Thus, MCT1 deficiency appeared dispensable for T_{reg} cell survival and function, although under highly inflammatory conditions they may have decreased activity.

However, we reasoned MCT1-mediated lactate uptake would be most important within lactate-rich tumor tissue. Inoculating *Slc16a1*$^{f/f}$*Foxp3*^{Cre} mice with B16 melanoma resulted in slowed tumor growth and prolonged survival (Fig. 4b). Characterizing the infiltrate when both genotypes harbored tumors of similar sizes (day 14) showed while CD8$^+$ T cells in *Slc16a1*$^{f/f}$*Foxp3*^{Cre} mice exhibited higher coinhibitory markers PD-1 and Tim-3, indicative of terminal differentiation (Fig. 4c), CD8$^+$ and T_{conv} cells were more proliferative and

competent to produce IFN-γ, suggesting decreased suppressive function by MCT1-deficient T_{reg} cells (Fig. 4d, e). Indeed, intratumoral MCT1-deficient T_{reg} cells had reduced suppressive function *ex vivo* (Fig. 4f) and were less proliferative, resembling intratumoral T_{reg} cells from 3MP-treated mice (Fig. 4g, 3k). Analysis of 3MP-treated *Slc16a1*$^{f/f}$*Foxp3*^{Cre} mice suggested 3MP's effects on T_{reg} cells was mediated through MCT1 (Extended Data Fig 3k,l). Characterization of intratumoral MCT1-deficient T_{reg} cells revealed decreases in CD44 and Nrp1 staining, concomitant with elevated PD-1 staining, potentially indicating dysfunctional T_{reg} cells[28] (Fig. 4h). Metabolically, MCT1-deficient, tumor-resident T_{reg} cells compensated by becoming glucose avid (Fig. 4i). We found, as a consequence, that MCT1-deficient T_{reg} cells would no longer persist within the lactate rich hypoxic areas of tumors, as measured by pimonidazole staining, despite overall tumor hypoxia remaining similar (Fig. 4j, Extended Data Fig. 4p).

To remove any unforeseen effects of MCT1 deletion on T_{reg} cell development, we interrupted MCT1 expression just prior to B16 melanoma injection using a tamoxifen-inducible, T_{reg} cell-specific model (*Slc16a1*$^{f/f}$*Foxp3*$^{Cre.ERT2}$) and showed similar immunologic and survival outcomes, including the development of a 'fragile'[29] T_{reg} cell phenotype in which Foxp3^{+} cells begin expressing IFN-γ (Extended Data Fig. 5). Induced T_{reg} deletion of MCT1 also slowed tumor growth of MC38 adenocarcinoma and MEER HNSCC (Fig. 4k, Extended Data Fig. 5g,h). We thus reasoned loss of lactate uptake in T_{reg} cells produced an environment conducive to immunotherapy. Triggering deletion of MCT1 in T_{reg} cells synergized with anti-PD-1 therapy, resulting in complete regressions in 37.5% of B16-bearing mice (typically insensitive to anti-PD-1) (Fig. 4l). Deletion of MCT1 from T_{conv} cells using *Slc16a1*$^{f/f}$*Cd4*^{Cre} mice did not impact their capacity to produce IL-2 and IFN-γ, suggesting MCT1 was not generally required for T cell function (Extended Data Fig 4q). Thus, MCT1 expression and consequent lactic acid uptake is dispensable for most tissue derived T_{reg} cells but required to maintain high suppressor activity in the TME.

Our study highlights the antagonistic effects of glucose on T_{reg} cell function and identity. While previous data support this[9,10,23,30], some studies using transcriptomic and proteomic analysis suggest T_{reg} cells are highly glycolytic[31–33]. We demonstrate T_{reg} glucose consumption is certainly heterogeneous between tissues (Fig. 1g) and within the T_{reg} population (Fig 2a); however, glucose uptake characterizes poorly suppressive T_{reg} cells, or at least those suppressing via mechanisms not potent *in vitro* coculture (Fig. 2a,c Extended Data Fig. 2a). Importantly, T_{reg} cells consuming low amounts of glucose still express glycolytic pathway genes (Fig. 2h). As most reactions in glycolysis are reversible, T_{reg} cells likely build higher-order intermediates from carbon sources like lactate (Fig. 3).

Lactate is often thought of as a waste product of glycolytic metabolism, but it represents an important metabolite for cellular function and a likely fuel source for tissues[20]. Our data suggest T_{reg} cells do not require lactic acid for survival, but are endowed with metabolic flexibility to use this carbon source, both as fuel and as a means to protect their high suppressive capacity from negative effects of glucose (Fig 3i). Consequently, cells do not possess both high lactic acid and glucose uptake (Fig 1g, 2f, 3c,d, Extended Data Figure 3d). Thus, we propose a glucose:lactate axis exists to fine-tune T_{reg} cell functioning depending on the nutrient milieu (Fig 2g, 3i). Lactate not only fuels the TCA cycle but is also exported

from the mitochondria, contributing to higher glycolytic pathways via PEP. This gluconeogenic component of lactate metabolism supports T_{reg} cell proliferation, critical in a cell type that does not readily take up glucose. However, the contribution of PEPCK-independent lactate metabolism appears also to be at the level of T_{reg} cell suppression (Fig. 4f), suggesting lactate plays a multi-pronged role in T_{reg} cell biology.

It is unlikely regulatory T cells evolved to thrive in tumors; rather cancers exploit this predilection for alternative substrates to maintain an immunosuppressive environment. Lactate is not only enriched in the tumor but is elevated in immunologically distinct tissue environments such as muscle, adipose, and nervous system[34,35]. We also suspect lactate is one of a host of alternative metabolites T_{reg} cells can utilize. MCT1 itself can also transport acetate, succinate, propionate, and butyrate, which have been shown to play roles in T_{reg} cells[21,36,37]. Indeed, our findings using transfer colitis suggest MCT1 deficiency may impact T_{reg} cell function in the gut. Notably, however, we did not observe overt gut inflammation at the steady state in *Slc16a1*$^{f/f}$*Foxp3*^{Cre} mice, suggesting both inflammation and MCT1 substrate availability play roles in maintaining T_{reg} cellsin that environment..

Our study suggests that, as T_{reg} cells must be active when immune activity is at its lowest, they exist metabolically ‘out-of-sync’ with their conventional counterparts. This requires utilizing fuels prevalent in tissue environments to maintain suppressor function when their conventional T cell targets may be competing for nutrients. As lactate can promote suppressive functions of other tolerogenic cell types, like tumor-associated macrophages[38], cell types sharing lactate metabolism may share suppressor activity. While this is exploited in the tumor microenvironment, causing suppressive cells to thrive, it is actionable: T_{reg} cell-specific deletion of the lactate transporter not only results in decreased tumor growth but synergy with checkpoint blockade immunotherapy. MCT1 inhibition to directly target lactate metabolism or inhibition of tumor acidity may break this metabolic symbiosis and lower the regulatory T cell barrier to cancer immunity.

MATERIALS AND METHODS

In Vitro Tissue Culture

B16-F10 were obtained from ATCC. MC38 cells were obtained from Dario Vignali (commercially available from Kerafast). Clone24 was originally produced by single cell sorting melanoma tumors arising from *Pten*$^{f/f}$*Braf*$^{LSL\text{-}V600E}$*Tyr*^{CreER} mice[5]. MEER cells were obtained from Robert Ferris (originally from [39]). B16 cell line was authenticated in 2018 by independent sequencing. MC38 cells were authenticated in 2016 by independent sequencing. Clone24 was authenticated via metabolic profiling and tumor growth compared to Melan-A (normal melanocytes) in 2019[5]. MEER cells were authenticated in 2013 via immunoblot to show E6/E7 and Ras overexpression in MTEC cells. MC38 and MEER were confirmed mycoplasma free in 2016, B16 were confirmed in 2018, Clone24 in 2019. Both primary and immortalized cell lines were maintained in lab-made R10 media [RPMI1640, 10%FBS, 2mM L-glut, PenStrep, NEAA, 1mM Sodium pyruvate, 5mM HEPES, β-ME]. Cultures were incubated in temperature and partial pressure-stable conditions at 37°C and 5% CO_2. For *in vitro* conditioning experiments, isolated T_{reg} or T_{conv} cells were activated in complete R10 media with 0.1 ug/mL Phorbol 12-myristate 13-acetate (PMA) and 1ug/mL

ionomycin (Sigma-Aldrich) with 1000U/mL IL-2 for ~20 hours at 37°C then placed in the conditions indicated in the figure with IL-2. For *in vitro* 3-mercaptopicolinic acid (3MP, Cayman Chemical) experiments a 250 μM concentration was used.

In Vivo Mice Studies

Sample sizes were not statistically predetermined but were chosen based on previous work in T_{reg} cell functional assays[8,29] and tumor immunology[4,5,8,14,29]. These sample sizes are sufficient because they allowed for the determination of statistical significance between groups and minimized the number of animals or replicates needed for each experiment. Mice were placed into experimental group by nature of their genotype and/or if receiving treatment were randomized within a genotype. For experiments not involving mice, cells were randomized into experimental groups. Blinding was not possible as most of the data acquisition and analysis was done by a single person; two individuals performing every experiment was not feasible during the course of our study. C57BL/6J-*Foxp3*^{YFPiCre}, -*Foxp3*$^{GFP.Cre.ERT2}$, -*Rag1*$^{-/-}$, and -*Thy1*^{a} (Thy1.1 congenic) were purchased from The Jackson Laboratory. *Slc16a1*$^{f/f}$ mice were a gift from Jeffrey Rothstein and Brett Morrison[40] used to generate *Slc16a1*$^{f/f}$*Foxp3*$^{GFP.Cre.ERT2}$ (termed *Slc16a1*$^{f/f}$*Foxp3*$^{Cre\text{-}ERT2}$*)* and *Slc16a1*$^{f/f}$*Foxp3*$^{YFP.Cre}$ (termed *Slc16a1*$^{f/f}$*Foxp3*^{Cre}*)* mice. *Foxp3*$^{\text{FlpO Ametrine}}$ mice were a gift from Dario AA Vignali. Spleens of OT-II Foxp3^{RFP} Thy1.1^{+} mice were a gift from Geoffrey Camirand. Animal work was done in accordance with the Institutional Animal Care and Use Committee of the University of Pittsburgh (protocol #17071235). All mice were housed in specific pathogen free conditions at an ambient temperature 20-26°C and humidity of 30-70% with a 12:12 hour light:dark cycle prior to use. The maximal tumor size of 15 mm in any direction was not exceed in any experiment. Both male and female mice were used in studies, from five (5) to ten (10) weeks of age.

Flow Sorting and Cytometric Analysis

Single-cell suspensions from murine tumors (day 14 post tumor inoculation), lymph node, liver, thymus, or spleen were derived through mechanical separation and 70 μM filter (Fisherbrand) passage. For hypoxia detection, mice were injected intravenously with pimonidazole (80mg/kg, Hypoxyprobe) in PBS 1.0 hour before sacrifice. Tumors dissolution was aided through lab-made tumor lysis buffer [2mg/mL Collagenase Type IV (Gibco), 2U/mL Dispase in Hanks' Balanced Salt Solution (Stemcell Technologies), 10U/mL Deoxyribonuclease I (Sigma), serum free RPMI medium] injected with a 20G needle and incubated for 30 minutes at 37°C. Prior to sort tumor suspensions were purified by negative selection with MojoSort magnetic bead separation (BioLegend) and biotin-conjugated anti-mouse antibodies to CD105 (MJ7/18, Cat# 120403, Lot# B266720, BioLegend).The skin (ears of mice were used), were finely minced using scissors and resuspended in RPMI1640 (Gibco, Grand Island, NY) with 2.5 mg/mL collagenase XI (Sigma-Aldrich), 0.25 mg/mL hyaluronidase (Sigma-Aldrich), 0.1 mg/mL DNase (Sigma-Aldrich), 0.01 M HEPES (Sigma-Aldrich), and 10% FBS followed by incubation in a shaking incubator for 1 h at 37C at 250 rpm. Following incubation skin was subjected to mechanical separation and passed through a 70 μM filter. Similarly, muscles (quadriceps were used) were finely minced using scissors then resuspended in 0.05% type II collagenase (ThermoFisher) in HBSS for 30 min at 37 °C under constant agitation. Islets were isolated as previously described[41].

Pimonidazole was visualized using anti-pimonidazole antibodies (Hypoxyprobe, Cat# HP7-100, Lot# 5914) after 5 minutes of 4% PFA fixation followed by the FoxP3 Fix/perm kit (Biolegend). Staining for expression markers was performed with anti-mouse specific antibodies obtaining from the following companies; Biolegend: anti-CD4 (GK1.5, Cat# 100412, Lot# B184560, dil 1:1000), CD8 (53-6.7, Cat# 100707, Lot# B171971, dil 1:1000), CD39 (Duha59, Cat# 143806, Lot# B186014, dil 1:500), CD44 (IM7, Cat# 103032, Lot# B267976, dil 1:500), CD73 (TY/11.8, Cat# 127215, Lot# B260585, dil 1:500), CD279 (PD-1, 29F.1A12, Cat# 135221, Lot# B194160, dil 1:250), HAVcr-2 (TIM-3, RMT3-23, Cat# 119705, Lot# B224472, dil 1:250), Helios (22F6, Cat# 137220, Lot# B155089, dil 1:250), IFNγ (XMG1.2, Cat# 505842, Lot# B270630, dil 1:250), Ki67 (16A8, Cat# 652403, Lot# B208445, dil 1:250), CD304 (Nrp-1, 3E12, Cat# 145212, Lot# B175814 dil 1:200), TNFα (MP6-XT22, Cat# 506322, Lot# B218553, dil 1:500). BD Horizon: CD62L (MEL-14, Cat# 564109, Lot# 7341887, dil 1:500). eBioscience: FoxP3 (FJK-16s, Cat# 53-5773-82, Lot#2011698, dil 1:250). Intracellular staining was performed using FoxP3 Fix/Perm buffer set (BioLegend) as per manufacturer's protocol and staining was performed on overnight at 4°C. Stained cells were analyzed on a LSRFortessa (BD). Cell doublets were excluded by comparison of side-scatter and forward-scatter width to area. Flow cytometry data and proliferation modeling were analyzed with FlowJo v10 software (Tree Star) and figures were produced in Prism v8 (GraphPad).

Glucose Uptake Assay

Single cell suspensions of tumor and lymph node and other tissues of ~1 million cells/mL were placed in serum free RPMI containing 40 μM 2NBDG or 0.4 μM Glucose-Cy5 for 25 minutes at 37°C. Glucose-Cy5, a Cy5-linked 1-amino-glucose tracer was synthesized in collaboration with Dr. Marcel Bruchez[17]. For OT-II experiments, $CD4^+$ T cells were isolated via negative selection using magnetic bead separation as previously described[4] then injected retroorbital into C57BL/6J mice. Simultaneously, recipient mice were injected I.P. with 1 x 10^6 vaccinia-OVA viral particles and harvested 5 days later.

Microsuppression & Proliferation Assays

In vitro microsuppression assays were performed as previously described[29]. Briefly T_{reg} cells ($CD4^+FoxP3^+$) populations were isolated via flow assisted sorting from tumor or lymph node from C57BL/6J-*Foxp3*$^{GFP.Cre.ERT2}$, -*Foxp3*$^{YFP.Cre}$ mice or mice crossed to these strains. Responder cells ($CD4^+Foxp3^-$ T_{conv}) and antigen presenting cells ($CD4^-CD8^-$ APCs) were isolated via flow assisted sorting from the spleen of a C57BL/6J-*Thy1*^{a} mouse. T_{reg} cells were co-cultured for 72 hours at 37°C with APCs and CellTrace Violet (CTV, ThermoFisher Scientific) labeled responder cells at ratios from 1:2 (T_{reg}:responder) to 1:32 in complete RPMI media with 1ug/mL anti-CD3. Proliferation assays were performed by labeling isolated T_{reg}, T_{conv}, and CD8 T cells with CTV then activating at 1 million cells/mL using anti-CD3/CD28 Dynabeads according to the manufacture's protocol (ThermoFisher Scientific) and IL-2 in complete RPMI media containing 0 to 10mM lactic acid (Fisher Bioreagents). Cell proliferation of responding cell populations was modeled using FlowJo v10 software (Tree Star).

RT-qPCR

Total RNA was extracted using Trizol reagent (Invitrogen) and cDNA was transcribed using a High Capacity cDNA Reverse Transcription Kit (Applied Biosystems), according to manufacturer protocol. Transcript levels were measured with SybrGreen (ThermoFisher Scientific) and using primers specific to genes of interest, including; *Slc16a1*: FWD 5'-GCAGTGTTAGTCGGAGCC-3' REV 5'-GCGATCATTACTGGACGGC-3', *Ldha*: FWD 5'-AGCTTCCATTTAAGGCCCCG-3' REV 5'-TCTTTTGAGACCGCTAGTGC-3' cDNA concentration was normalized per samples relative to β-actin. All experiments were performed in technical triplicates.

Cytokine Production Assay

Cell suspensions were stimulated in complete R10 media with 0.1 ug/mL Phorbol 12-myristate 13-acetate (PMA) and 1ug/mL ionomycin (Sigma-Aldrich) for ~20 hours at 37°C. Five hours prior to antibody staining, Golgi-Plug (BD Biosciences) was added to the samples. Cells were surfaced stained and then intracellular stained using FoxP3 Fix/Perm buffer set (Invitrogen) as per manufacturer's protocol. Unstimulated controls were used to determine gating strategies.

Interstitial Lactate Quantification

Tumor and spleen were harvested and placed in empty 15mL conical tubes. Tissues were cut up with scissors then wrapped with a 5-micron Nylon filter paper (Sterlitech) and stuffed filter down into a 1.5 mL conical tube making sure the tissue did not touch the bottom. Tissues were centrifuged at 4000 rpm for 2 hours. Interstitial fluid was assayed for L-lactate concentration using a colorimetric detection kit according to manufacturer's protocol (abcam).

Isotopic Flux Analysis

Cell suspensions at 1 million cells/mL in complete RPMI media were stimulated for 24 hours at 37°C with plate-bound anti-mouse CD3ε (10 μg for Treg, 3 μg for Tconv, clone 145-2C11, Cat#100239, Lot# B306297, Biolegend) and soluble anti-mouse CD28 (2 μg/mL, clone 37.51, Cat#102115, Lot#B283231, Biolegend) and IL-2 (1000U/mL T_{reg} 50U/mL T_{conv}). After activation media was exchanged for complete RPMI with 5mM uniformly labeled ^{13}C-L-Lactate (Sigma Aldrich) and IL-2. For some experiments PEPCK inhibitor, 3-mercaptopicolinic acid (3MP, Cayman Chemical) was added at 250 μM. Media was then titrated to pH 6.88 with 1 N HCl. Suspensions were pulsed for 25 hours then washed 2x with room temperature PBS then resuspended in ice cold 80% methanol.

Metabolic quenching and polar metabolite pool extraction was performed using ice cold 80% methanol in water with 0.1% formic acid at a ratio of 400μL per 100μL. Deuterated (D4)-taurine and (D3)-lactate (Sigma-Aldrich) was added to the sample lysates as an internal standard for a final concentration of 100μM. The supernatant was cleared of protein by centrifugation at 16,000xg. 5μL of cleared supernatant was subjected to online LC-MS analysis.

Analyses were performed by untargeted LC-HRMS. Briefly, Samples were injected via a Thermo Vanquish UHPLC and separated over a reversed phase Phenomenex Kinetex C18+ column (2.1×100mm, 1.7μm particle size) maintained at 40°C. For the 20 minute LC gradient, the mobile phase consisted of the following: solvent A (1.5mM ammonium fluoride) and solvent B (100% acetonitrile). The gradient was the following: 0-12.0 min 5% B, to 1000% B, 12.0-15.0 min hold at 100% B, 15.0-15.1100% to 5% B, 15.1-20.0 min 5%B. The Q Exactive mass spectrometer was operated in polarity switching mode, using both positive and negative ion mode, scanning in Full MS mode (2 μscans) from 66.7 to 1000 m/z at 70,000 resolution with an AGC target of 3e6. Source ionization settings were 4.5/3.0 kV spray voltage respectively for positive and negative mode. Source gas parameters were 20 sheath gas, 10 auxiliary gas at 250°C, and 4 sweep gas. Calibration was performed prior to analysis using the PierceTM Positive and Negative Ion Calibration Solutions (Thermo Fisher Scientific). Integrated peak areas were then extracted manually using Quan Browser (Thermo Fisher Xcalibur ver. 2.7). Fully untargeted analysis was completed by using Thermo Compound Discoverer 3.0 software suite to extract and align molecular features. Graphs and statistical analyses (either t-test or ANOVA) were prepared with GraphPad Prism 7.0 (GraphPad Software, Inc., La Jolla, CA, USA).

In Vivo Tumor Growth and Therapy

Slc16a1$^{f/f}$*Foxp3*^{Cre} *or Foxp3*^{Cre} mice were inoculated with 1.5 x 10^5 B16-F10 cells in complete RPMI media. To monitor tumor growth, tumors area was determined 3x weekly using digital calipers and stopped once tumors reached 15mm in any direction. For 3MP treated mice, *Foxp3*^{Cre} *or Foxp3*$^{Cre.ERT2}$ mice were inoculated with 1.5 x 10^5 B16-F10 cells. Starting on day 10 or 12 post tumor inoculation mice were treated daily either with water or 25 mg/kg 3MP (Caymen Chemical) via intraperitoneal (I.P.) injection. On day 14 one hour prior to sacrifice, mice were given a final dose of 25 mg/kg 3MP or water. For 3MP tumor growth, treatment started day 7 post tumor injection and continued daily with 25 mg/kg 3MP or H_2O I.P. until tumors reached 15mm in any direction.

For the inducible deletion of MCT1 (*Slc16a1*) *Slc16a1*$^{f/f}$*Foxp3*$^{GFP.Cre.ERT2}$ or *Foxp3*$^{GFP.Cre.ERT2}$ mice were treated I.P. or P.O. with 1 mg of tamoxifen (T5648, Sigma) in corn oil (C8267, Sigma) from day −4 to 0. On day 0, mice were inoculated intradermally with 2.5x10^5 B16-F10, MC38, or MEER cells in complete RPMI media and given a dose of 1mg Tamoxifen. Tamoxifen treatment continued 3x weekly until the conclusion of the experiment. On day 7, when tumors reached 1-10 mm^2 mice were treated with 0.2mg anti–PD-1 or hamster IgG isotype control (Bio X Cell) 3x weekly until the conclusion of the experiment.

pHrodo Red Lactic Acid Uptake Assay

Cell suspensions from lymph nodes and day 14 B16-F10 tumors were loaded with pHrodo Red AM (ThermoFisher Scientific) according to manufacturer's protocol in a 20mM HEPES in PBS solution. Cells were surfaced stained for multicolor flow cytometry following the normal protocol in 20mM HEPES/PBS buffer. At the flow cytometer, lactic acid was spiked into each sample at a final concentration of 5mM pH ~6.7. Samples were read at 0, 10, and 30 mins after addition of lactic acid.

Extracellular flux analysis

Isolated T_{reg} and T_{conv} cells were plated on Cell-Tak coated Seahorse culture plates (250,000/well) in media consisting of minimal, unbuffered DMEM supplemented with 2mM glutamine. Basal rates were taken for 30 min, and then streptavidin-complexed anti-$CD3^{biotin}$ at 3 μg/mL was injected and readings continued for 3 hrs. 2μM oligomycin and 10mM 2-DG were injected to obtain maximal and minimal ECAR values, respectively. Similarly, isolated T_{reg} and T_{conv} cells were activated using plate bound anti-CD3 (5 μg/mL) and soluble anti-CD28 (2 μg/mL) with 250 U/mL IL-2 for 48hrs then plated on Cell-Tak coated Seahorse culture plates (100,000/well) in media consisting of minimal, unbuffered DMEM supplemented with 2mM glutamine. Basal extracellular acidification rates were taken for 30 mins. Cells were stimulated with 10mM Glucose, 2μM oligomycin, 10mM 2-DG.

Transfer Colitis

The transfer colitis model was performed as previously described[42]. Briefly, $2NBDG^{hi}$ and $2NBDG^{lo}$ T_{reg} cells from Foxp3-Ametrine reporter mice or T_{reg} cells from *Slc16a1*$^{f/f}$*Foxp3*^{Cre} or *Foxp3*^{Cre} were isolated via flow assisted sorting (CD4-APC^+ Foxp3-reporter$^+$). T_{conv} cells ($CD4^+$ $CD25^-$) from C57BL/6J-*thy1*^{a} were isolated via flow assisted sorting. Rag1$^{-/-}$ mice were simultaneously given 2 x 10^4 sorted T_{reg} cells and 1 x 10^5 thy1.1$^+$ T_{conv} cells via retroorbital injection. Mice were weighed once a week for 7 weeks (experiment end). Sections of colons were fixed in 10% formalin and paraffin embedded. Slides were stained with hematoxylin and eosin by the University of Pittsburgh Pathology Department, and histology scores were blindly determined using criteria previously described[42].

Tumor Histology

After pimonidazole pulsing, tumors were dissected and frozen at -80 deg C in Optimal Cutting Temperature Compound (OCT) (Tissue-Tek) and sectioned (Cryostat microtome). Tissue was fixed in histology-grade acetone (Fisher) at −20 deg C, then rehydrated in staining buffer, stained with hypoxyprobe (Hypoxyprobe, catalog# HP7-100Kit), and DAPI (Life Technologies), and mounted with ProLong Diamond AntifadeMountant (Life Technologies). Sections were imaged with an Olympus IX83 microscope and analyzed with ImageJ and NIS-Elements Imaging Software.

RNA Sequencing

1000 low glucose and high glucose consuming T_{reg} cells were sorted directly into lysis buffer in a 96-well plate. Immediately after sorting cDNA was generated using SMART-seq HT kit (Cat # 634456 Clontech) using 1000 cells. cDNA product was checked by Tape Station D5000 from Agilent technologies 2200 to make sure cDNA was successfully generated. Library construction was done using Nextrera XT kit # 15031942 from Illumina. 1ng cDNA was used in total volume 5ul. Sequencing was done using NextSeq 500 System. High Output 75 Cycles kit with run Parameter Paired Read 150 cycles (2X75).

Sequencing reads were trimmed for adapters using Cutadapt[43] prior to being aligned to Mus musculus reference genome (mm10) using the RNA-seq aligner HISAT2. Subread's

featureCounts function was used for gene level quantification and results were normalized to Transcripts Per Kilobase Million (TPM). Using the raw quantification, differential genes were found with the R package DESeq2 and statistical cutoffs of q-value <0.05 and |log2foldchange|>1.5.

Statistical Analysis

The data presented in the figures are mean ± standard error of the mean (S.E.M.). Multiple group comparison in *in vivo* and *ex vivo* assays was accomplished with one- or two-way analysis of variance (ANOVA). For single comparison, unpaired two-tailed Student's t test was used, unless otherwise denoted. In cases of non-Gaussian distribution, nonparametric t-test was used. Survival and tumor growth in *in vivo* implantable tumor models are presented as Kaplan–Meier survival curves and plotted tumor area with respect to time and were statistically analyzed using log rank test. All analysis was completed with on Prism v5 software (GraphPad). A value of $P < 0.05$ is statistically significant. In the figures, standard designations of significance were given; *$p < 0.05$; **$p < 0.01$; ***$p < 0.001$ and ****$p < 0.0001$. The specific analysis used per figure in the manuscript can be found within the legends.

Data availability

RNA sequencing data that support the findings of this study (Fig. 2b, h) have been deposited in GEO with the GSE158801 accession code. The authors declare that the data supporting the findings of this study are available within the paper and its supplementary information files.

Extended Data

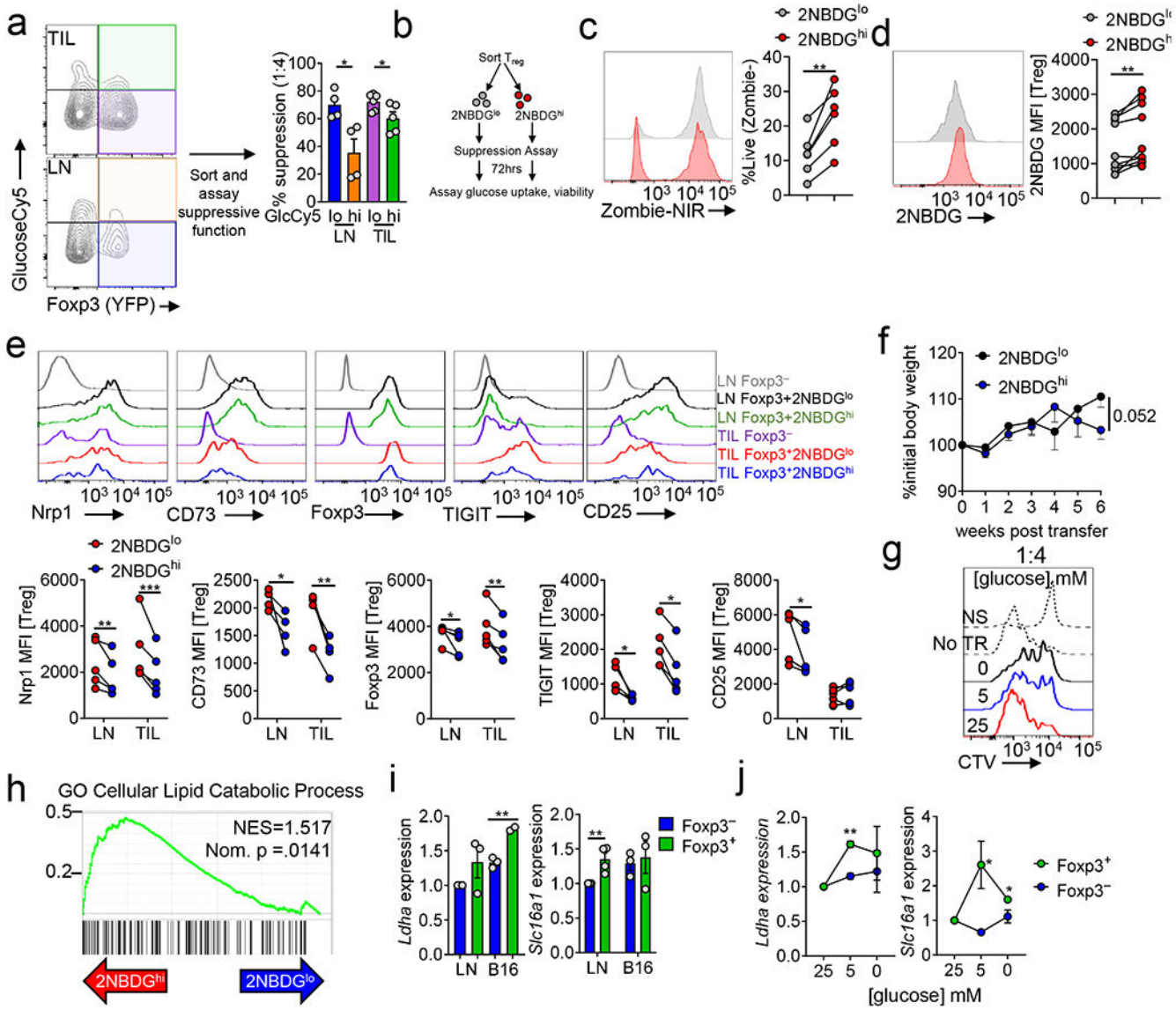

Extended Data Figure 1. 1-amino-Cy5-glucose (GlucoseCy5) can act as a surrogate for 2NBDG in GFP/YFP T_{reg} reporter mice.

(**a**) Gating strategy for T_{reg} and T_{conv} cells (**b**) Representative plot of percent T_{reg} ($CD4^+Foxp3^+$) in the lymph node (LN) and tumor (TIL) of B16 bearing C57BL/6 mice day 14 post tumor inoculation. Representative plots gated on total $CD4^+$ cells. (**c**) Glycolytic extracellular acidification rates (ECAR) of T_{reg} and T_{conv} cells sorted from LN and B16 TIL preparations as in (b) 48hrs after activation with αCD3/CD28 and IL-2. Oligo = oligomycin, 2-DG = 2-deoxy-D-glucose, ΔECAR = max reading after glucose minus basal ECAR. Max ECAR = max reading at after oligo minus basal ECAR. (**d**) *Ex vivo* 2NBDG uptake mean fluorescence intensity (MFI) by T_{reg}, T_{conv}, and $CD8^+$ T cells from the LN and B16 TIL (**p=0.0045). (**e**) *Ex vivo* 2NBDG uptake by $CD44^+CD62L^-$ and $CD44^-CD62L^+$ T_{reg} and T_{conv} cells isolated from the LN of Foxp3-Ametrine reporter mice. (**f**) Lymphocytes from

Foxp3-Ametrine reporter mice were simultaneously pulsed with 2NBDG and GlucoseCy5. Representative plot is gated $CD4^+$ $Foxp3^+$ with tabulation of percent $GlucoseCy5^+$ of $2NBDG^+$ T_{reg}. (**g**) *Ex vivo* GlucoseCy5 uptake by $CD44^+$ T_{reg} and T_{conv} cells from the LN and B16 TIL. Representative plots gated on $CD44^+$ $CD4^+$ cells (**p=0.0025). (**h**) GlucoseCy5 positivity in Nrp1 negative and positive T_{reg} cells. (**i**) *Ex vivo* GlucoseCy5 uptake by T_{conv} cells isolated from various tissues. Results are representative of three (a-d,f-i) or two (e) independent experiments. Significance (*p< 0.05, **p <0.01, ***p < 0.001, ****p<0.0001) was determined by paired two-tailed t test (e), unpaired two-tailed t test (d,f,g,h) or two-way ANOVA with Sidak's multiple comparisons test (c). Data are mean values of biological replicates ±SEM.

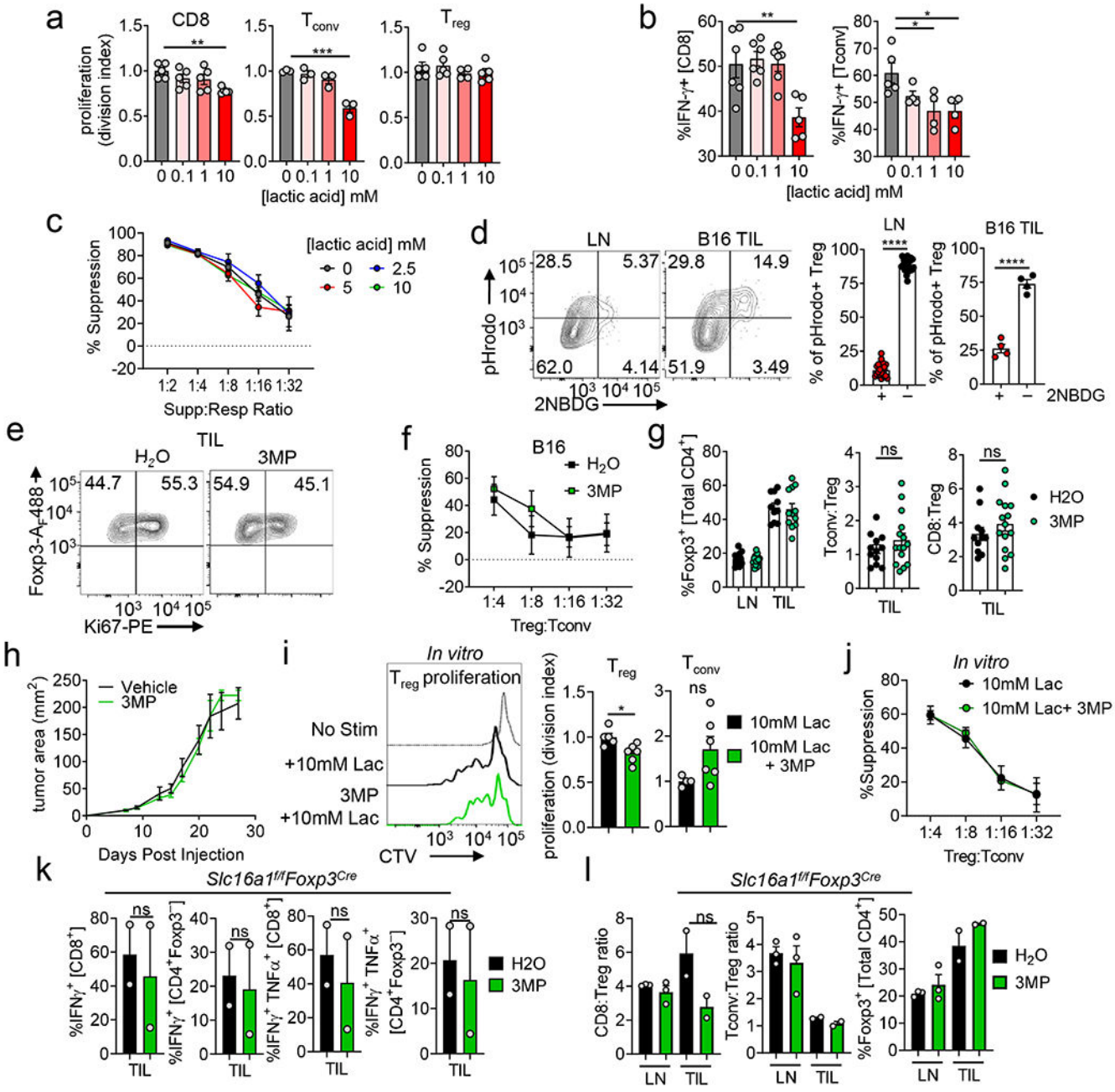

Extended Data Figure 2. Glucose avid T_{reg} cells harbor a weaker T_{reg} cell signature but retain viability and some suppressor activity.

(**a**) T_{reg} cells were sorted based on GlucoseCy5 uptake and assayed for their ability to suppress the proliferation of CellTrace Violet (CTV) labeled T_{conv} cells at 1:4 (Treg:Tconv) (LN*p=0.02, TIL *p=0.041). (**b**) Experimental diagram for (c, d). (**c**) Representative histogram and quantification of viability of sorted 2NBDG^{hi} and 2NBDG^{lo} T_{reg} cells after 72hrs in a suppression assay. (**d**) 2NBDG uptake by 2NBDG^{hi} or 2NBDG^{lo} T_{reg} as in (b). (**e**) Representative histograms and tabulation of T_{reg} signature gene expression between 2NBDG low and high T_{reg} cell subsets (Nrp1 **p=0.0016, CD73 *p=0.029 **p=0.0076,

TIGIT LN*p=0.04 TIL*p=0.016, CD25 *p=0.037). (**f**) Weights of *Rag1*$^{-/-}$ mice that received an adoptive transfer of either 2NBDG^{lo} or 2NBDG^{hi} T_{reg} cells plus Thy1.1^{+} T_{conv} cells I.V. (**g**) Representative histogram of T_{conv} responder cell proliferation after 72hrs of co-culture with T_{reg} cells (1:4) conditioned in 0, 5, or 25mM glucose for 3 days. The suppression assay occurred in 25 mM glucose conditions. (**h**) Geneset enrichment plot of cellular lipid catabolic process from TIL 2NBDG^{hi} vs 2NBDG^{lo} T_{reg} cells. (**i**) mRNA expression of *Slc16a1* and *Ldha* in LN- and B16-infiltrating T_{reg} and T_{conv} cells by qPCR (*Ldha* **p=0.004, *Slc16a1* **p=0.009). (**j**) *Slc16a1* and *Ldha* mRNA expression in T_{reg} or T_{conv} cells activated overnight and conditioned in the glucose concentration indicated for 3 days (normalized to 25mM glucose, significance between T_{reg} and T_{conv}) (*Ldha* **p=0.002 *Slc16a1* 5 *p=0.030, 0 *p=0.046). Results are representative of three (a,e,h,i,j), or two (c,d,f) independent experiments. Significance (*p< 0.05, **p <0.01, ***p < 0.001) determined by unpaired two-tailed t test (a,f,i,j) or paired two-tailed t test (c,d) or two-way ANOVA with Sidak's multiple comparisons test (e). Data are mean values of biological replicates ±SEM.

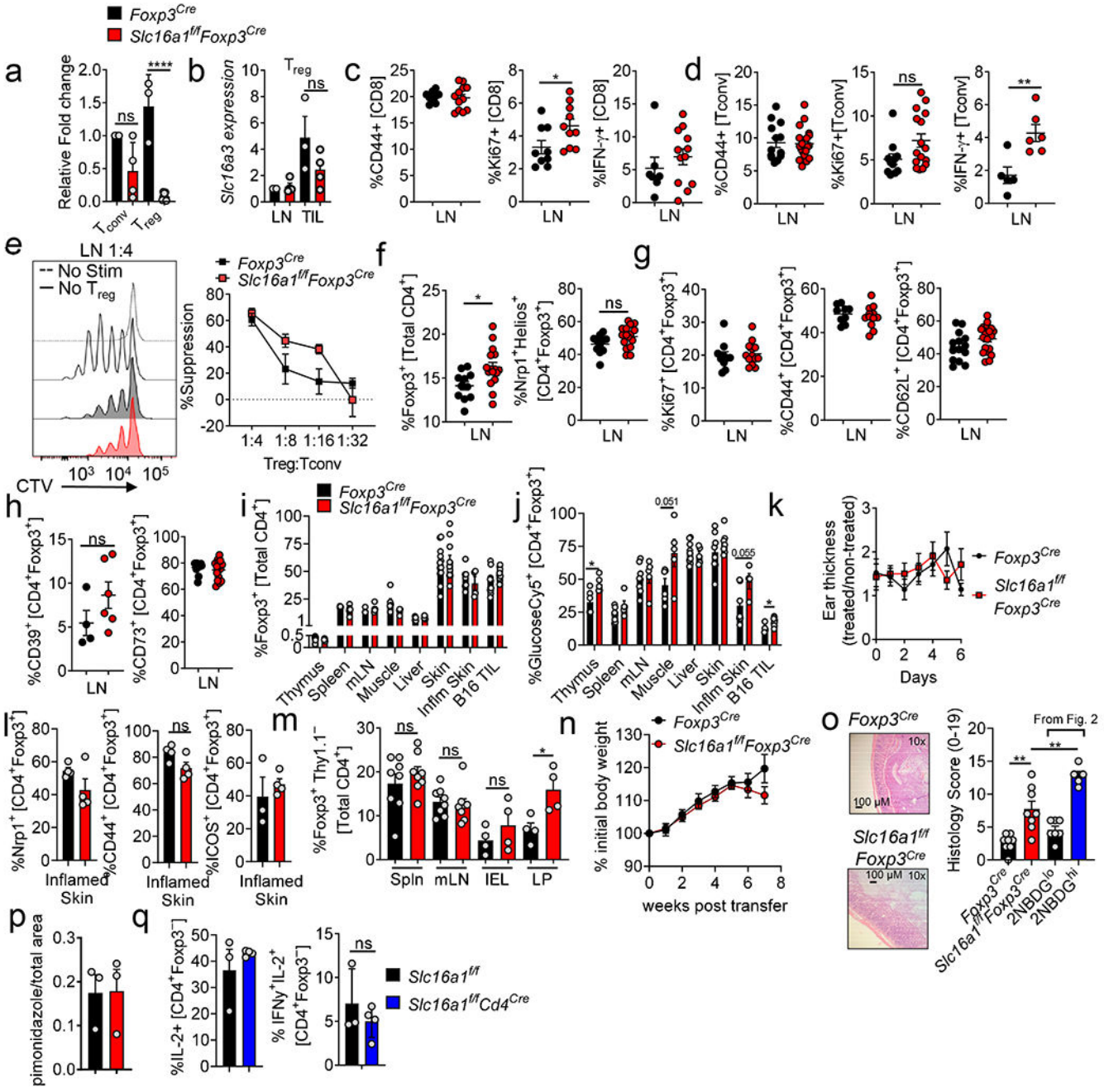

Extended Data Figure 3. T_{reg} cells are resistant to lactic acid and use PEPCK-mediated metabolic pathways to support their proliferation.

(**a**) Proliferation of $CD8^+$, T_{conv}, and T_{reg} cells labeled with CellTrace Violet (CTV) activated in media with lactic acid for 3 days (**p=0.0058). (**b**) IFN-γ production of CD8 and T_{conv} cells conditioned as in (a) then restimulated overnight with PMA/ionomycin (CD8 **p=0.0042, Tconv *p=0.02). (**c**) Suppression assay using T_{reg} cells conditioned as in (a) performed in absence of additional lactic acid. (**d**) Representative histogram and quantification of $pHrodo^+$ T_{reg} cells taking up 2NBDG. (**e**) Representative flow plot of Ki67 expression by B16-infiltrating T_{reg} cells from mice treated ±3MP for 3 days. (**f**) Suppressive

capacity of T_{reg} cells, isolated from mice as in Fig.3k. (**g**) Percent Foxp3$^+$ cells, T_{conv}:T_{reg} ratio, and CD8:T_{reg} ratio within the TIL of mice treated as in (f). (**h**) Tumor growth curve of B16 in C57BL/6 mice treated with H_2O or 3MP. (**i**) Proliferation of T_{reg} and T_{conv} cells activated and cultured in 10mM lactic acid media ±3MP for 3 days (*p=0.016). (**j**) Capacity of activated T_{reg} cells conditioned in 10mM lactic acid media ± 250μM 3MP for 3 days to suppress the proliferation of CTV labelled T_{conv} cells. (**k**) IFN-γ expression by CD8 and T_{conv} cells in *Foxp3^{Cre}* or *Slc16a1$^{f/f}$Foxp3^{Cre}* mice treated as in (f). (**l**) Percent Foxp3$^+$ cells, T_{conv} to T_{reg} ratio, and CD8 to T_{reg} ratio within LN and tumor of *Slc16a1$^{f/f}$Foxp3^{Cre}* mice treated as in (f). Results are representative of four (d), three (a,b,c,f,g,i), or two (h,j,k,l) independent experiments. Significance (*p< 0.05, **p <0.01, ***p < 0.001, ****p<0.0001) determined by unpaired two-tailed t test (d,e,g,i,k,l) or one-way ANOVA with Dunnett's multiple comparisons test (a,b) or two-way ANOVA with Sidak's multiple comparisons test (c,f,h,j). Data are mean values of biological replicates ±SEM.

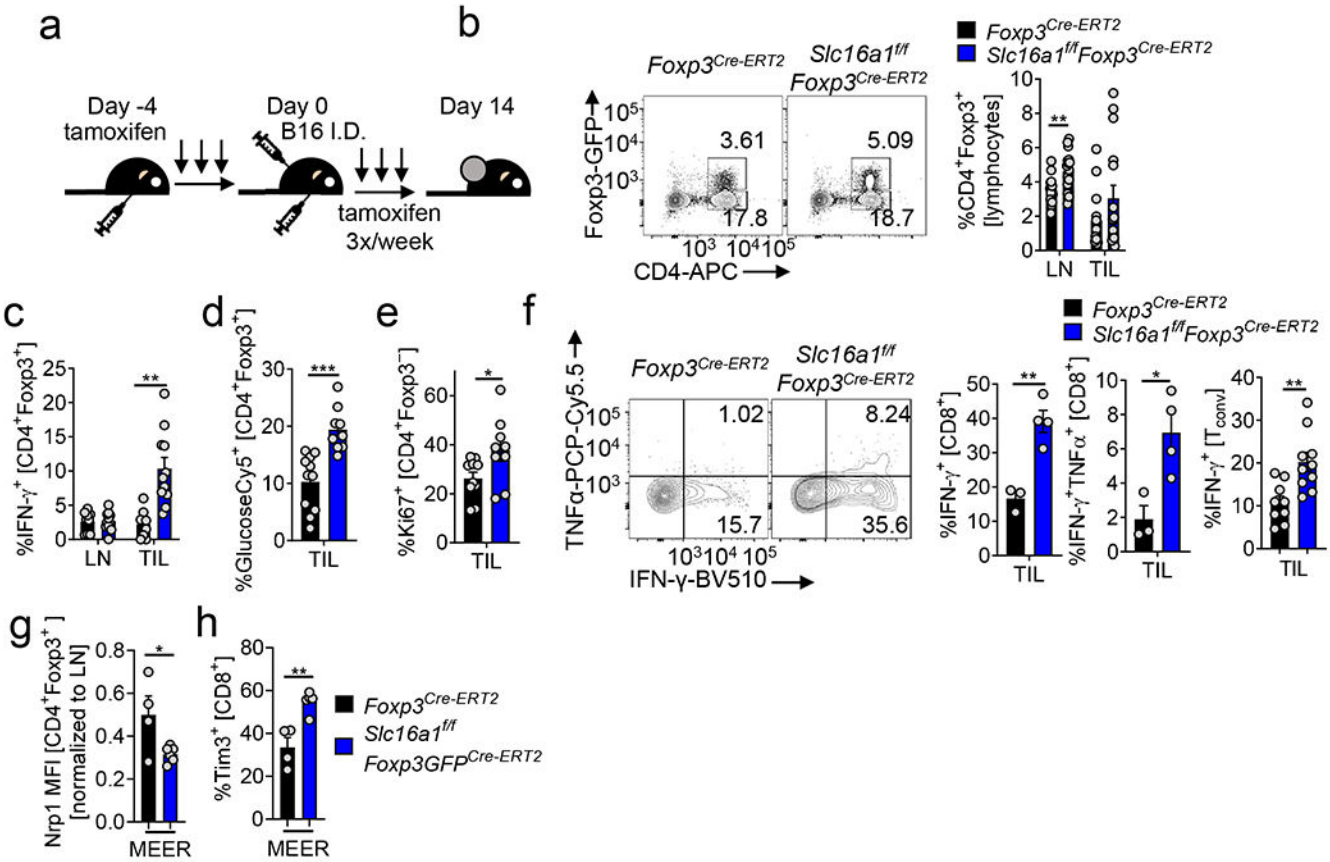

Extended Data Figure 4. MCT1 is efficiently deleted in T_{reg} cells of *Slc16a1$^{f/f}$Foxp3$^{YFP-Cre}$* mice and is not required for peripheral T_{reg} cell function.

(**a**) *Slc16a1* expression in T_{conv} and T_{reg} cells from the lymph nodes (LN) of *Foxp3^{Cre}* or *Slc16a1$^{f/f}$Foxp3^{Cre}* mice. (**b**) T_{reg} cell mRNA expression of *Slc16a3* (MCT4) from mice as in (a). CD44, Ki67, and IFN-γ production by LN CD8$^+$ T cells (**c**, *p=0.039) or T_{conv} cells (**d**, **p=0.007) from mice as in (a). (**e**) Capacity of LN-derived T_{reg} cells as in (a) to suppress proliferation of CellTrace Violet (CTV) labelled T_{conv} cells. (**f**) Percent Foxp3$^+$ and

Nrp1^{+}Helios^{+} LN T_{reg} cells from mice as in (a) (*p=0.013). (**g**) CD44, Ki67, and CD62L expression by LN T_{reg} cells as in (a). (**h**) CD39 and CD73 expression by LN T_{reg} cells as in (a). Percent of Foxp3^{+} cells (**i**) or GlucoseCy5^{+} T_{reg} cells (**j**) from various tissues of mice as in (a) (thymus *p=0.014, B16 *p=0.019). (**k**) Normalized ear thickness of imiquimod treated mice as in (a). (**l**) Percent marker positive T_{reg} cells from mice treated as in (k). (**m**) Foxp3 expression in transferred wild type or *Slc16a1*-deficient T_{reg} infused with Thy1.1^{+} T_{conv} cells into *Rag1*$^{-/-}$ mice iv. (*p=0.02) (**n**) Weight of *Rag1*$^{-/-}$ mice over time from (m). (**o**) Representative sections of the colon and quantified histology scores 7 weeks post transfer from mice as in (m) and Fig.2d (**p=0.001, **p=0.009). (**p**) Anti-pimonidazole area over tumor area (B16) calculated from immunofluorescence from *Foxp3*^{Cre} and *Slc16a1*$^{f/f}$*Foxp3*^{Cre} mice. (**q**) IL-2 and IFN-γ expression by *Slc16a1*-deficient T_{conv} cells stimulated overnight with PMA/ionomycin. Results are representative of four (c,d,f,g), three (a,b,e,h,j,p,q), or two (k,l,m,i,o) independent experiments. Significance (*p< 0.05, **p <0.01, ****p < 0.0001) determined by unpaired two-tailed t test (a-d,f-q) or two-way ANOVA (e). Data presented as mean values of biological replicates ±SEM.

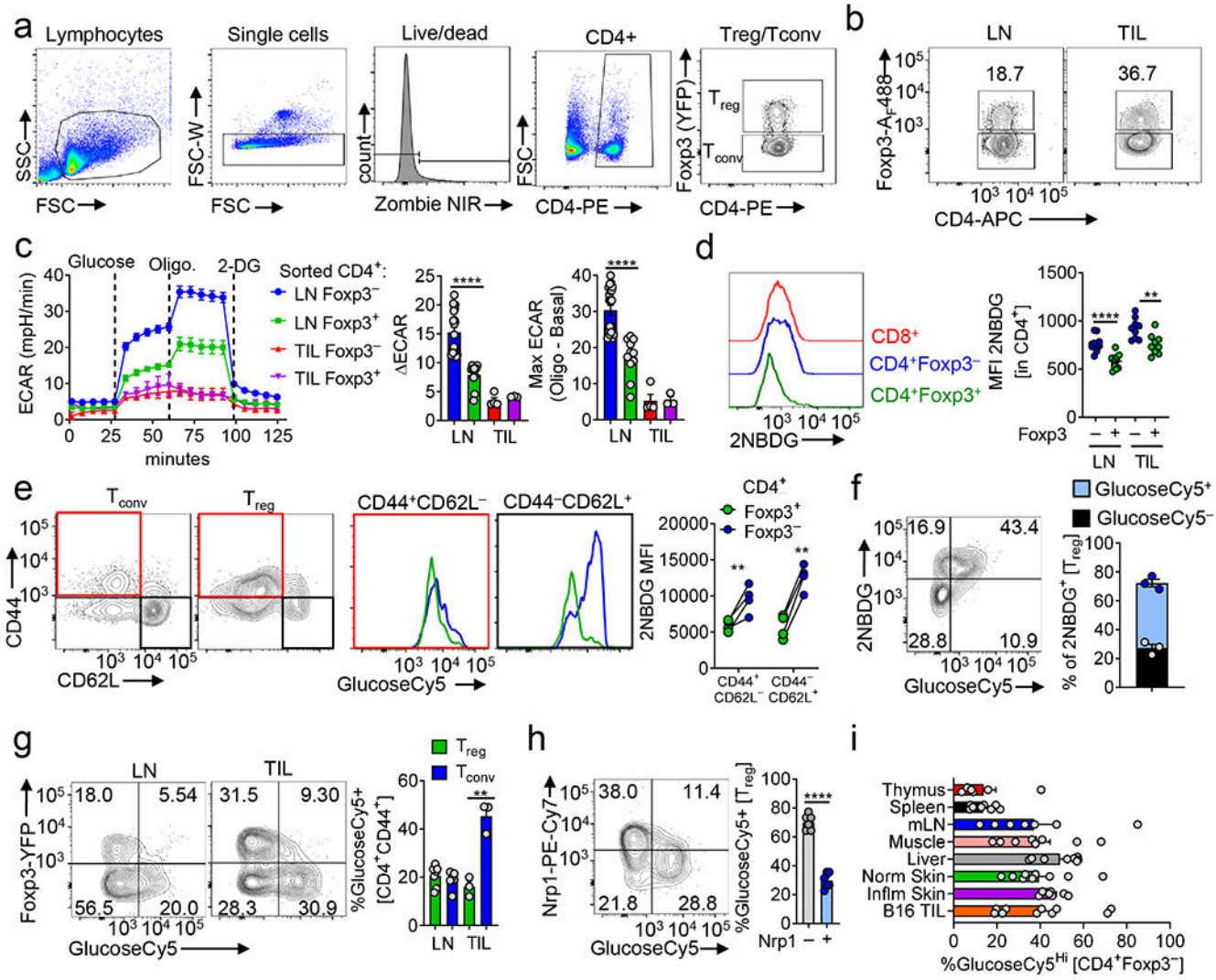

Extended Data Figure 5. Acute deletion of MCT1 results in similar immunologic phenotypes in B16 melanoma and predilection towards a fragile T_{reg} cell phenotype.

(**a**) *Foxp3*$^{Cre\text{-}ERT2}$ and *Slc16a1*$^{f/f}$*Foxp3*$^{Cre\text{-}ERT2}$ mice were treated 5 consecutive days with tamoxifen I.P. prior to inoculation with 1.5 x 10^5 B16 tumor cells. Following inoculation, tamoxifen was administered I.P. 3 times a week until sacrifice at day 14. (**b**) Percent Foxp3$^+$ CD4$^+$ cells in the lymph node (LN) and tumor (TIL) as in (a) (**p=0.005). (**c**) Tabulation of IFN-γ production by T_{reg} cells from the LN and TIL of mice as in (a) (**p=0.002). (**d**) Glucose consumption by T_{reg} cells from the TIL of mice as in (a). (**e**) Percent proliferating T_{conv} cells from the TIL of mice as in (a) (*p=0.037). (**f**) Representative flow plot and tabulation of IFN-γ and TNFα production by CD8 T cells from the TIL of mice as in (a) (**p=0.003, *p=0.02). Tabulation of IFN-γ production by T_{conv} cells from the TIL of mice as in (a) (**p=0.003). (**g**) Nrp1 mean fluorescence intensity on MEER intratumoral Treg cells derived from *Foxp3*$^{Cre\text{-}ERT2}$ and *Slc16a1*$^{f/f}$*Foxp3*$^{Cre\text{-}ERT2}$ mice treated as in (a) (*p=0.034). (**h**) Tim-3 expression by MEER derived CD8 T cells from mice as in (g) (**p=0.003). Results are representative of four (b,c,d,e), or three (f), or two (g,h)

independent experiments. Significance (*p< 0.05, **p <0.01) determined by unpaired two-tailed t test (b-h). Data presented as mean values of biological replicates ±SEM.

Acknowledgements

The authors wish to thank Amanda Burton and Creg Workman for the generation and gift of the *Foxp3*$^{\text{FlpO-Ametrine}}$ mice and Geoffrey Camirand for the gift of OT-II Foxp3$^{\text{RFP}}$ Thy1.1^{+} spleens. This work was supported by the Sidney Kimmel Foundation, an NIH Director's New Innovator Award (DP2AI136598), the Hillman Fellows for Innovative Cancer Research Program, a Stand Up to Cancer-American Association for Cancer Research Innovative Research Grant (SU2C-AACR-IRG-04-16), the Alliance for Cancer Gene Therapy, the UPMC Hillman Cancer Center Skin Cancer and Head and Neck Cancer SPOREs (P50CA121973 and P50CA097190), the Mark Foundation for Cancer Research's Emerging Leader Award, a Cancer Research Institute's Lloyd J. Old STAR Award, and the Sy Holzer Endowed Immunotherapy Fund (all to G.M.D.). D.A.A.V is supported by R01DK089125, R01CA203689 and P01AI108545. Trainees on this manuscript were supported by T32CA082084 (to M.J.W., P.D.A.V., A.E.O.D., and K.D.), F31AI149971 (to M.J.W.), F30CA247034 (to P.D.A.V.), (F31CA247129 to K.D.), T32AI089443 (to R.M.P and S.G.), F31AI147638 (to S.G.), and a Damon Runyon Cancer Research Fellowship (A.E.O.D.). Mass spectrometry was supported by S10OD023402 (to S.G.W.), and floxed animal generation was supported by R01NS099320 (to J.D.R., and B.M.M). as well as R01 NS086818 (to B.M.M.). Synthesis of Glucose-Cy5 was supported by R21AI135367 (to G.M.D.). Sequencing was supported by the Samuel and Emma Winters Foundation and a Grand Prize Award Grant (2017) from the Immuno-Oncology Young Investigators' Forum (both to G.M.D.) and was performed at the University of Pittsburgh Health Sciences Sequencing Core at Children's Hospital of Pittsburgh. RNA sequencing analysis was supported in part by the University of Pittsburgh Center for Research Computing through the resources provided. This work utilized the UPMC Hillman Cancer Center Flow Cytometry and Animal Facilities, supported in part by P30CA047904.

Bibliography

1. Wang H, Franco F & Ho P-C Metabolic regulation of tregs in cancer: opportunities for immunotherapy. Trends Cancer 3, 583–592 (2017). [PubMed: 28780935]
2. Sakaguchi S, Yamaguchi T, Nomura T & Ono M Regulatory T cells and immune tolerance. Cell 133, 775–787 (2008). [PubMed: 18510923]
3. Hanahan D & Weinberg RA Hallmarks of cancer: the next generation. Cell 144, 646–674 (2011). [PubMed: 21376230]
4. Scharping NE et al. The tumor microenvironment represses T cell mitochondrial biogenesis to drive intratumoral T cell metabolic insufficiency and dysfunction. Immunity 45, 374–388 (2016). [PubMed: 27496732]
5. Najjar YG et al. Tumor cell oxidative metabolism as a barrier to PD-1 blockade immunotherapy in melanoma. JCI Insight 4, (2019).
6. Ho P-C et al. Phosphoenolpyruvate Is a Metabolic Checkpoint of Anti-tumor T Cell Responses. Cell 162, 1217–1228 (2015). [PubMed: 26321681]
7. Wang D et al. Targeting EZH2 reprograms intratumoral regulatory T cells to enhance cancer immunity. Cell Rep. 23, 3262–3274 (2018). [PubMed: 29898397]
8. Delgoffe GM et al. Stability and function of regulatory T cells is maintained by a neuropilin-1-semaphorin-4a axis. Nature 501, 252–256 (2013). [PubMed: 23913274]
9. Michalek RD et al. Cutting edge: distinct glycolytic and lipid oxidative metabolic programs are essential for effector and regulatory CD4+ T cell subsets. J. Immunol. 186, 3299–3303 (2011). [PubMed: 21317389]
10. Gerriets VA et al. Foxp3 and Toll-like receptor signaling balance T reg cell anabolic metabolism for suppression. Nat. Immunol 17, 1459 (2016). [PubMed: 27695003]
11. Weinberg SE et al. Mitochondrial complex III is essential for suppressive function of regulatory T cells. Nature 565, 495–499 (2019). [PubMed: 30626970]
12. Rubtsov YP et al. Regulatory T cell-derived interleukin-10 limits inflammation at environmental interfaces. Immunity 28, 546–558 (2008). [PubMed: 18387831]
13. Rubtsov YP et al. Stability of the regulatory T cell lineage in vivo. Science 329, 1667–1671 (2010). [PubMed: 20929851]

14. Menk AV et al. Early TCR signaling induces rapid aerobic glycolysis enabling distinct acute T cell effector functions. Cell Rep. 22, 1509–1521 (2018). [PubMed: 29425506]
15. Lunt SY & Vander Heiden MG Aerobic glycolysis: meeting the metabolic requirements of cell proliferation. Annu. Rev. Cell Dev. Biol 27, 441–464 (2011). [PubMed: 21985671]
16. Single cell glucose uptake assays: A cautionary tale. Immunometabolism (2020). doi:10.20900/immunometab20200029
17. Xu H et al. Cyanine-based 1-amino-1-deoxyglucose as fluorescent probes for glucose transporter mediated bioimaging. Biochem. Biophys. Res. Commun 474, 240–246 (2016). [PubMed: 27033602]
18. Chang C-H et al. Posttranscriptional control of T cell effector function by aerobic glycolysis. Cell 153, 1239–1251 (2013). [PubMed: 23746840]
19. D'Alise AM, Ergun A, Hill JA, Mathis D & Benoist C A cluster of coregulated genes determines TGF-beta-induced regulatory T-cell (Treg) dysfunction in NOD mice. Proc. Natl. Acad. Sci. USA 108, 8737–8742 (2011). [PubMed: 21543717]
20. Hui S et al. Glucose feeds the TCA cycle via circulating lactate. Nature 551, 115–118 (2017). [PubMed: 29045397]
21. Halestrap AP & Wilson MC The monocarboxylate transporter family--role and regulation. IUBMB Life 64, 109–119 (2012). [PubMed: 22162139]
22. Romero-Garcia S, Moreno-Altamirano MMB, Prado-Garcia H & Sánchez-García FJ Lactate contribution to the tumor microenvironment: mechanisms, effects on immune cells and therapeutic relevance. Front. Immunol 7, 52 (2016). [PubMed: 26909082]
23. Angelin A et al. Foxp3 Reprograms T Cell Metabolism to Function in Low-Glucose, High-Lactate Environments. Cell Metab. 25, 1282–1293.e7 (2017). [PubMed: 28416194]
24. Fischer K et al. Inhibitory effect of tumor cell-derived lactic acid on human T cells. Blood 109, 3812–3819 (2007). [PubMed: 17255361]
25. Liu C et al. Lactate inhibits lipolysis in fat cells through activation of an orphan G-protein-coupled receptor, GPR81. J. Biol. Chem 284, 2811–2822 (2009). [PubMed: 19047060]
26. Jackson VN & Halestrap AP The kinetics, substrate, and inhibitor specificity of the monocarboxylate (lactate) transporter of rat liver cells determined using the fluorescent intracellular pH indicator, 2',7′-bis(carboxyethyl)-5(6)-carboxyfluorescein. J. Biol. Chem 271, 861–868 (1996). [PubMed: 8557697]
27. Robinson BH & Oei J 3-Mercaptopicolinic acid, a preferential inhibitor of the cytosolic phosphoenolpyruvate carboxykinase. FEBS Lett. 58, 12–15 (1975). [PubMed: 1225570]
28. Lowther DE et al. PD-1 marks dysfunctional regulatory T cells in malignant gliomas. JCI Insight 1, (2016).
29. Overacre-Delgoffe AE et al. Interferon-γ Drives Treg Fragility to Promote Anti-tumor Immunity. Cell 169, 1130–1141.e11 (2017). [PubMed: 28552348]
30. Macintyre AN et al. The glucose transporter Glut1 is selectively essential for CD4 T cell activation and effector function. Cell Metab. 20, 61–72 (2014). [PubMed: 24930970]
31. Li L et al. TLR8-Mediated Metabolic Control of Human Treg Function: A Mechanistic Target for Cancer Immunotherapy. Cell Metab. 29, 103–123.e5 (2019). [PubMed: 30344014]
32. Procaccini C et al. The proteomic landscape of human ex vivo regulatory and conventional T cells reveals specific metabolic requirements. Immunity 44, 406–421 (2016). [PubMed: 26885861]
33. Priyadharshini B et al. Cutting Edge: TGF-β and Phosphatidylinositol 3-Kinase Signals Modulate Distinct Metabolism of Regulatory T Cell Subsets. J. Immunol 201, 2215–2219 (2018). [PubMed: 30209190]
34. Consoli A, Nurjhan N, Reilly JJ, Bier DM & Gerich JE Contribution of liver and skeletal muscle to alanine and lactate metabolism in humans. Am. J. Physiol 259, E677–84 (1990). [PubMed: 2240206]
35. Proia P, Di Liegro CM, Schiera G, Fricano A & Di Liegro I Lactate as a metabolite and a regulator in the central nervous system. Int. J. Mol. Sci 17, (2016).
36. Arpaia N et al. Metabolites produced by commensal bacteria promote peripheral regulatory T-cell generation. Nature 504, 451–455 (2013). [PubMed: 24226773]

37. Smith PM et al. The microbial metabolites, short-chain fatty acids, regulate colonic Treg cell homeostasis. Science 341, 569–573 (2013). [PubMed: 23828891]

38. Colegio OR et al. Functional polarization of tumour-associated macrophages by tumour-derived lactic acid. Nature 513, 559–563 (2014). [PubMed: 25043024]

39. Jung Y-S et al. CD200: association with cancer stem cell features and response to chemoradiation in head and neck squamous cell carcinoma. Head Neck 37, 327–335 (2015). [PubMed: 24700450]

40. Jha MK et al. Monocarboxylate transporter 1 in Schwann cells is critical for maintenance of sensory nerve myelination during aging. BioRxiv (2019). doi:10.1101/686832

41. Lennon GP et al. T cell islet accumulation in type 1 diabetes is a tightly regulated, cell-autonomous event. Immunity 31, 643–653 (2009). [PubMed: 19818656]

42. Ostanin DV et al. T cell transfer model of chronic colitis: concepts, considerations, and tricks of the trade. Am. J. Physiol. Gastrointest. Liver Physiol 296, G135–46 (2009). [PubMed: 19033538]

43. Martin M Cutadapt removes adapter sequences from high-throughput sequencing reads. EMBnet j. 17, 10 (2011).

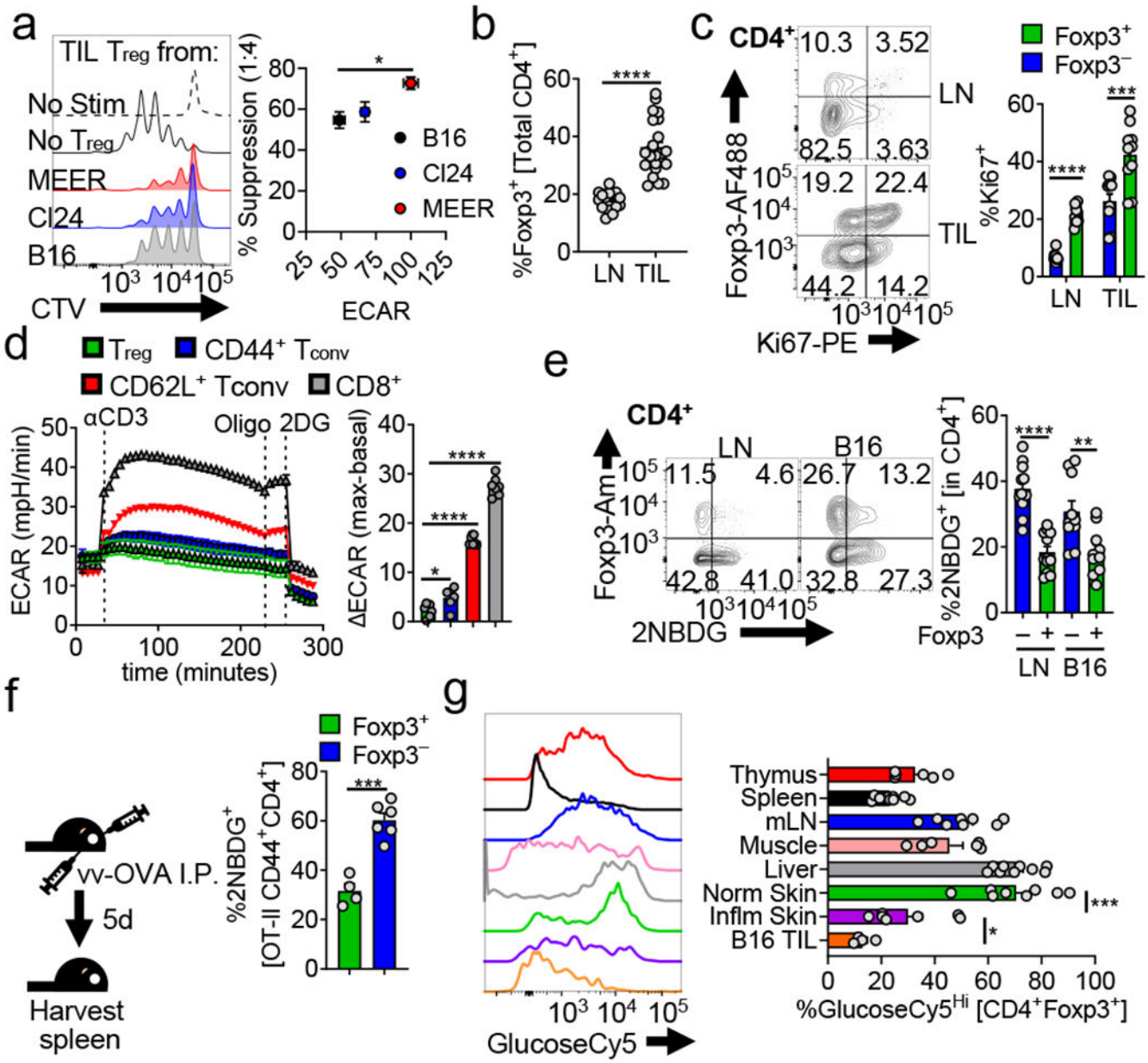

Figure 1. Regulatory T cells possess a distinct metabolic profile from conventional T cells in normal and transformed tissues.

(**a**) (left) Representative histogram of T_{conv} responder cell proliferation dye dilution after 72hrs of co-culture with T_{reg} cells isolated from B16, Cl24 (melanoma), or MEER (HPV+ HNSCC) tumors. (right) Capacity of T_{reg} cells to suppress the proliferation of CellTrace Violet (CTV) labelled T_{conv} cells as a function of the glycolytic extracellular acidification rate (ECAR) of the tumors from which they were isolated (*p=0.047). (**b**) Percent T_{reg} cells ($CD4^+$ $Foxp3^+$) of total $CD4^+$ T cells from lymph node (LN) and tumor infiltrating lymphocyte (TIL) preparations from C57BL/6 mice bearing B16 melanoma tumors (14 d post intradermal injection) (**c**) Percent proliferating ($Ki67^+$) T_{reg} and T_{conv} cells ($CD4^+$ $Foxp3^-$) from mice as in (b). (**d**) ECAR of in-Seahorse activated T_{reg}, CD8+, CD44+CD62L

− and CD44-CD62L+ T_{conv} cells sorted from LN and spleen of *Foxp3* reporter mice. Oligo = oligomycin, 2-DG = 2-deoxy-D-glucose, ΔECAR = max reading after αCD3 minus basal ECAR. (*p=0.022) (**e**) Flow cytogram depicting *ex vivo* 2NBDG uptake by T_{reg} and T_{conv} cells from the LN and B16 TIL of *Foxp3* reporter mice. Representative plots gated on CD4+ cells. (**p=0.006) (**f**) Diagram of experimental procedure and quantification of *ex vivo* 2NBDG uptake by $CD44^+$ OT-II T_{reg} and T_{conv} cells isolated 5 days after transfer into congenically mismatched hosts infection with Vaccinia-OVA. (**g**) Representative histogram and quantification of *ex vivo* GlucoseCy5 uptake by T_{reg} cells isolated from various tissues (*p=0.047). Results are representative of five (b), three (a,c,e, and g) or two (d,f) independent experiments. (*p< 0.05, **p <0.01, ***p < 0.001 ****p<0.0001) by unpaired two-tailed t test (a,b,d,f,g) or two-way ANOVA with Sidak's multiple comparisons test (c,e). Data are mean values of biological replicates ±SEM.

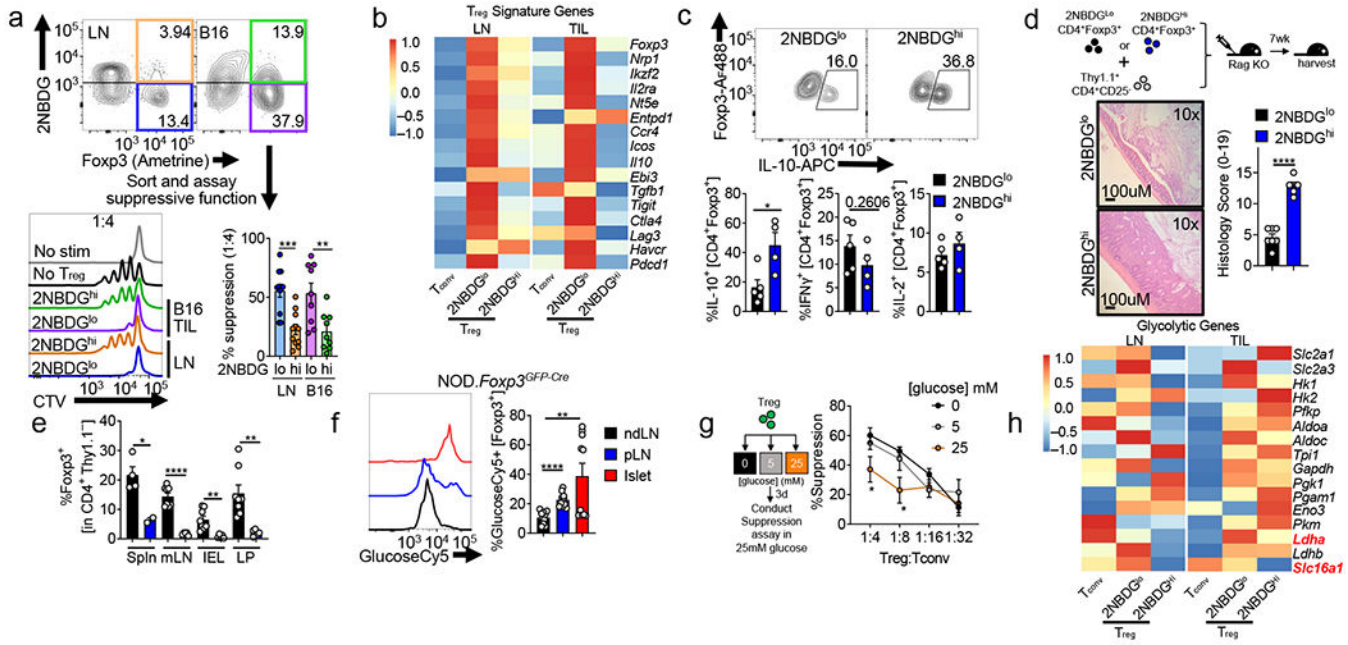

Figure 2. Glucose avidity is associated with reduced T_{reg} cell functional identity.

(**a**) Flow cytogram of CD4+ T cells from B16-bearing *Foxp3*^{Ametrine} mice depicting sorting strategies for T_{reg} cells based on their glucose uptake. T_{reg} cells sorted based on 2NBDG uptake were assayed for their ability to suppress the proliferation of CellTrace Violet (CTV) labeled T_{conv} cells. Representative histogram shows 1:4 ratio of T_{reg}:T_{conv}. (**p=0.0056). (**b**) T_{reg} cell signature gene expression in RNAseq analysis of 2NBDG^{hi} or 2NBDG^{lo} T_{reg} cells sorted from lymph node (LN) or tumor (TIL) of B16 melanoma-bearing *Foxp3* reporter mice as in (a). (**c**) Production of IL-10, IFN-γ, and IL-2 by sorted 2NBDG^{lo} and 2NBDG^{hi} T_{reg} cells stimulated overnight with PMA/ionomycin and stained intracellularly (*p=0.02). (**d**) Diagram and colon histology *Rag1*$^{-/-}$ mice that received either 2NBDG^{lo} or 2NBDG^{hi} Thy1.2^{+} T_{reg} cells plus Thy1.1^{+} T_{conv} cells I.V and followed for 7 wks. (**e**) Percent of transferred 2NBDG^{lo} or 2NBDG^{hi} T_{reg} cells as in (d) expressing Foxp3 within the spleen (Spln), mesenteric lymph node (mLN), intraepithelial layer (IEL), and lamina propria (LP) (*p=0.02, **p=0.004). (**f**) Representative histogram and tabulation of GlucoseCy5 uptake by T_{reg} cells isolated from the non-draining lymph node (ndLN), pancreatic lymph node (pLN), and the islet of 10-12-week-old NOD.*Foxp3*$^{GFP-Cre}$ mice (**p=0.005). (**g**) (left) Diagram of experimental procedure and (right) capacity of T_{reg} cells conditioned in 0,5, or 25mM glucose media to suppress the proliferation of CellTrace Violet (CTV) labelled T_{conv} cells. (1:4 *p=0.031, 1:8 *p=0.012 between 0 and 25 mM). (**h**) Glycolytic pathway gene expression as in (b). Results are representative of three (a,b,c,g,h), or two (d,e,f) independent experiments. Significance (*p< 0.05, **p <0.01, ***p < 0.001, ****p<0.0001) was determined by unpaired two-tailed t test (a,c,d,e,f), or two-way ANOVA with Tukey's multiple comparison test (g). Data are mean values of biological replicates ±SEM.

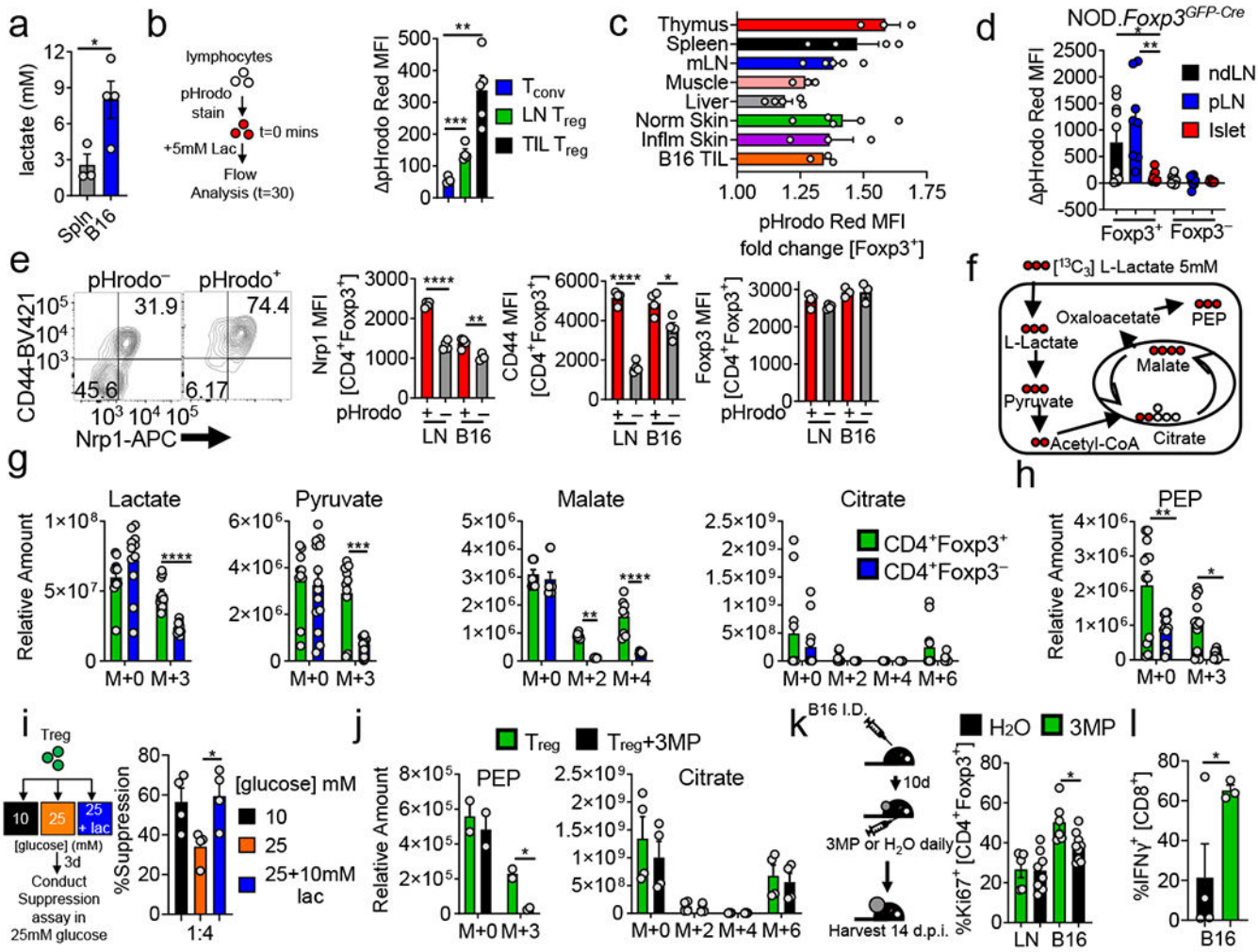

Figure 3. T_{reg} cells metabolize lactic acid to support their proliferation and suppressor function.

(**a**) Lactate concentration in spleen or B16 melanoma interstitial fluid (*p=0.041). (**b**) Lymphocytes from *Foxp3*^{Cre} mice were loaded with pHrodo Red (intracellular pH dye) and pulsed with 5mM lactic acid. Results are change of MFI from t=0 (**p=0.0012). (**c**) Lactic acid uptake determined as in (b) by T_{reg} cells infiltrating various tissues. (**d**) Lactic acid uptake from T_{reg} and T_{conv} cells isolated from islets, non-draining (ndLN), and pancreatic lymph node (pLN) of 10-12-week-old NOD.*Foxp3*$^{GFP-Cre}$ mice (*p=0.017, **p=0.001). (**e**) Flow cytogram and tabulation depicting Nrp1 and CD44 expression in T_{reg} cells based on lactate-elicited pH change (*p=0.018, **p=0.0097). (**f**) Diagram showing incorporation of ^{13}C derived from lactate into downstream metabolites. (**g**) Relative abundance determined by mass spectrometry of intracellular lactate, pyruvate, malate, and citrate in T_{reg} and T_{conv} cells activated overnight then pulsed with uniformly labeled ^{13}C-lactate (m+n equal to the number of incorporated heavy carbons) (**p=0.0025). (**h**) Relative abundance of PEP derived from ^{13}C-lactate as in (g) (*p=0.036, **p=0.0011). (**i**) Capacity of T_{reg} cells conditioned for 3 days in 25mM glucose media ±10mM lactic acid to suppress the proliferation of CellTrace Violet (CTV) labelled T_{conv} cells (*p=0.021). (**j**) As in (h) with the addition of PEPCK inhibitor 3MP (*p=0.018). (**k**) Ki67 expression in intratumoral T_{reg}

cells of B16 tumor-bearing mice treated with 3MP or water for 3 days (*p=0.015). (**l**) IFN-γ expression by B16-infiltrating $CD8^+$ T cells from mice treated as in (k) for 5 days. Results are representative of three (a,c,e,g,h,k), or two (b,d,i,j,l) independent experiments. Significance (*p< 0.05, **p <0.01, ***p < 0.001, ****p<0.0001) determined by unpaired two-tailed t test (a,b,d,e,i,j,k,l) or unpaired one-tail t test (l) or two-way ANOVA with Sidak's multiple comparisons test (g,h). Data are mean values of biological replicates ±SEM.

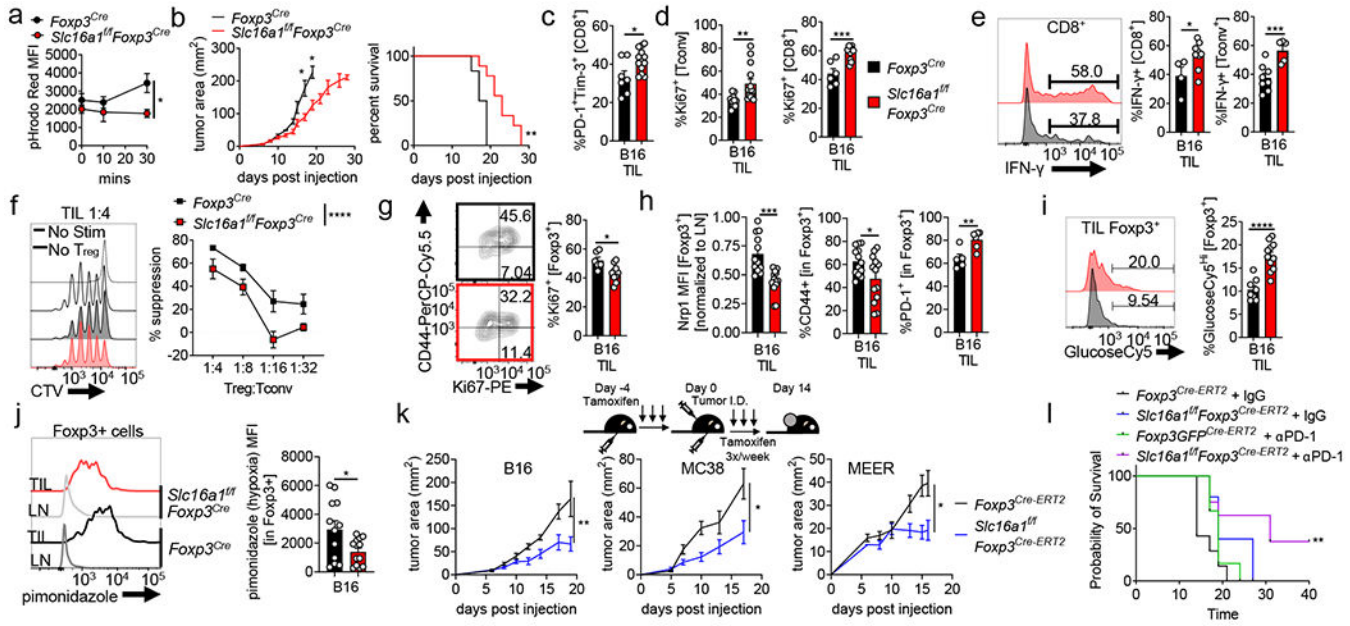

Figure 4. Tumor-infiltrating T_{reg} cells require lactate uptake to maintain their high suppressive function.

(**a**) Lactate-elicited pHrodo fluorescence in *Foxp3*^{Cre} or *Slc16a1*$^{f/f}$*Foxp3*^{Cre} T_{reg} cells (*p=0.041). (**b**) B16 tumor growth and survival of *Foxp3*^{Cre} and *Slc16a1*$^{f/f}$*Foxp3*^{Cre} mice (*p=0.0235) (**c**) Percent of B16-infiltrating PD-1^{+}Tim-3^{+} CD8^{+} T cells day 14 post tumor injection in mice as in (a) (*p=0.017). (**d**) Proliferation of tumor infiltrating T_{conv} and CD8^{+} T cells as in (c) (**p=0.009). (**e**) Tumor-infiltrating CD8^{+} and T_{conv} cells restimulated with PMA/ionomycin and stained for IFN-γ (*p=0.039). (**f**) Capacity of WT or *Slc16a1*-deficient tumor-infiltrating T_{reg} cells to suppress proliferation of CTV labeled T_{conv} cells. (**g**) Percent proliferating tumor infiltrating T_{reg} cells from mice as in (c). (*p=0.011). (**h**) Percent or MFI of WT and *Slc16a1*-deficient T_{reg} cells expressing Nrp1, PD-1, CD44 from B16 tumors (TIL) as in (c) (*p=0.029, **p=0.009). (**i**) GlucoseCy5 uptake by B16 tumor-infiltrating T_{reg} cells as in (c) (**j**) Pimonidazole staining of WT and *Slc16a1*-deficient T_{reg} cells from B16 tumors as in (c) (*p=0.029). (**k**) Tumor growth of B16 (melanoma, **p=0.0011) MC38 (adenocarcinoma, *p=0.023), and MEER (HNSCC, *p=0.0146) in tamoxifen treated *Foxp3*$^{Cre\text{-}ERT2}$ and *Slc16a1*$^{f/f}$*Foxp3*$^{Cre\text{-}ERT2}$ mice. Mice were given tamoxifen 5 consecutive days prior to tumor injection then 3x per week. (**l**) Survival of tamoxifen treated *Foxp3*$^{Cre\text{-}ERT2}$ and *Slc16a1*$^{f/f}$*Foxp3*$^{Cre\text{-}ERT2}$ mice injected with B16 and treated with IgG or anti-PD-1 antibodies 3x weekly (**p=0.002). Results are representative of four (b,c,d,f,g,h(Nrp1, CD44),i,j), three (a, k(B16)), or two (h(PD-1), k(MC38, MEER),l) independent experiments. Significance (*p< 0.05, **p <0.01, ***p < 0.001, ****p<0.0001) determined by the log-rank test for survival curves (b,l) or unpaired two-tailed t test (a,c,d,e,g,h,i,j) or two-way ANOVA (b,f,k). Data are mean values of biological replicates ±SEM.